

Functionalization of Ti6Al4V Alloy with Polyphenols: The Role of the Titanium Surface Features and the Addition of Calcium Ions on the Adsorption Mechanism

Original

Functionalization of Ti6Al4V Alloy with Polyphenols: The Role of the Titanium Surface Features and the Addition of Calcium Ions on the Adsorption Mechanism / Reggio, C., Barberi, J., Ferraris, S., Spriano, S.. - In: METALS. - ISSN 2075-4701. - 13:8(2023). [10.3390/met13081347]

Availability:

This version is available at: 11583/2981669 since: 2023-09-05T11:21:27Z

Publisher:

Multidisciplinary Digital Publishing Institute (MDPI)

Published

DOI:10.3390/met13081347

Terms of use:

This article is made available under terms and conditions as specified in the corresponding bibliographic description in the repository

Publisher copyright

(Article begins on next page)



Energy dependence of exclusive J/ψ photoproduction off protons in ultra-peripheral p–Pb collisions at $\sqrt{s_{NN}} = 5.02$ TeV

ALICE Collaboration*

CERN, 1211 Geneva 23, Switzerland

Received: 25 September 2018 / Accepted: 30 March 2019
© CERN for the benefit of the ALICE collaboration 2019

Abstract The ALICE Collaboration has measured the energy dependence of exclusive photoproduction of J/ψ vector mesons off proton targets in ultra-peripheral p–Pb collisions at a centre-of-mass energy per nucleon pair $\sqrt{s_{NN}} = 5.02$ TeV. The e^+e^- and $\mu^+\mu^-$ decay channels are used to measure the cross section as a function of the rapidity of the J/ψ in the range $-2.5 < y < 2.7$, corresponding to an energy in the γp centre-of-mass in the interval $40 < W_{\gamma p} < 550$ GeV. The measurements, which are consistent with a power law dependence of the exclusive J/ψ photoproduction cross section, are compared to previous results from HERA and the LHC and to several theoretical models. They are found to be compatible with previous measurements.

1 Introduction

One of the most interesting aspects of perturbative Quantum Chromodynamics (pQCD) is the evolution of the structure of hadrons in terms of quarks and gluons towards the high-energy limit [1]. Very precise measurements at HERA [2,3] have shown that the gluon structure function in protons rises rapidly at small values of the Bjorken x variable, which corresponds to the high-energy limit of QCD. This rise, interpreted as the growth of the probability density function for gluons, has to be damped at some high energy to satisfy unitarity constraints [4]. Although gluon saturation [5] is the most straightforward mechanism to slow down the growth of the cross section, no compelling evidence for this effect has been found so far. Gluon saturation would have important implications in small- x physics and in the early stages of ultra-relativistic heavy-ion collisions at RHIC and LHC; consequently, finding evidence for gluon saturation has become a central task for present experiments and for future projects [6,7].

The exclusive photoproduction of charmonium off protons ($\gamma p \rightarrow J/\psi p$) is a very clean probe with which to search for

saturation effects, because the cross section for this process depends, at leading order in pQCD, on the square of the gluon density in the target [8]. The mass of the charm quark provides a scale large enough to allow calculations within pQCD. A reduction in the growth rate of the cross section for this process as the centre-of-mass energy of the photon-target system increases would signal the onset of gluon saturation effects.

This process has been extensively studied in ep interactions at the HERA collider. Both ZEUS and H1 measured the energy dependence of exclusive J/ψ photoproduction off protons at γp centre-of-mass energies, $W_{\gamma p}$, from 20 to 305 GeV [9–11]. H1 has also measured exclusive $\psi(2S)$ photoproduction off protons with $W_{\gamma p}$ between 40 and 150 GeV [12].

The exclusive photoproduction of charmonium can also be studied at hadron colliders, where one of the incoming hadrons is the source of the photons and the other the target. CDF measured exclusive J/ψ production at mid-rapidities in $p\bar{p}$ collisions at the Tevatron [13], while LHCb reported measurements of exclusive J/ψ and $\psi(2S)$ production at forward rapidities in pp collisions at the LHC [14]. In addition, Υ production has been studied, both at HERA [15–17] and in pp collisions at the LHC [18]. In all cases, the experimental signature is the production of a vector meson in a collision in which there is no other hadronic activity, apart from the possible emission of a few very forward neutrons.

In hadron colliders, as the incoming particles can each be both source or target, there are two possible centre-of-mass energies for the photon-target system. This ambiguity can be resolved if the contribution of one beam acting as the source is much stronger than the other. This is the case for p–Pb collisions, because photon emission grows with the square of the electric charge and thus emission by the Pb ion is strongly enhanced with respect to that from the proton. ALICE published the first measurement of exclusive photoproduction of J/ψ , at forward and backward rapidities, in p–Pb collisions at the LHC [19].

* e-mail: alice-publications@cern.ch

In this Letter we present the measurements of exclusive J/ψ photoproduction in collisions of protons with Pb nuclei at a centre-of-mass energy per nucleon pair $\sqrt{s_{NN}} = 5.02$ TeV. The measurements are performed in the semi-backward ($-2.5 < y < -1.2$), mid ($|y| < 0.8$) and semi-forward ($1.2 < y < 2.7$) rapidity intervals, where the rapidity y of the J/ψ is measured in the laboratory frame with respect to the direction of the proton beam. The value of $W_{\gamma p}$ is determined by the rapidity of the J/ψ according to $W_{\gamma p}^2 = 2E_p M_{J/\psi} \exp(-y)$, where $M_{J/\psi}$ is the J/ψ mass and $E_p = 4$ TeV is the energy of the proton beam. Thus, the measurements presented here span the $W_{\gamma p}$ range from 40 to 550 GeV. Together with the measurements presented in [19] (for the rapidity ranges $-3.6 < y < -2.6$ and $2.5 < y < 4$), ALICE data map the $W_{\gamma p}$ dependence of the cross section for this process from about 20 to 700 GeV, which, using the standard definition $x = M_{J/\psi}^2 / W_{\gamma p}^2$, corresponds to three orders of magnitude, from $\sim 2 \times 10^{-2}$ to $\sim 2 \times 10^{-5}$.

2 Experimental set-up

The ALICE detector and its performance are described in detail in [20,21]. It consists of two main sections: a central barrel placed in a large solenoid magnet ($B = 0.5$ T), covering the pseudorapidity region $|\eta| < 0.9$, and a muon spectrometer covering the range $-4.0 < \eta < -2.5$. In addition, the analyses presented here make use of two other detector systems, V0 and ZDC, which are placed near the beam pipe and cover large pseudorapidities.

Because the proton and Pb beams had different energies, 4 TeV and 1.58 TeV per nucleon respectively, the nucleon-nucleon centre-of-mass was shifted, with respect to the laboratory frame, by $\Delta y_{NN} = 0.465$ in the direction of the proton beam. Collisions were performed in two configurations, denoted by p–Pb and Pb–p below, by reversing the directions of the LHC beams. According to the naming convention the *first* named particle (e.g. ‘p’ in p–Pb) is the one where the beam travels from the interaction region towards the muon spectrometer. Note that the convention in ALICE is that the pseudorapidity is negative in the direction of the muon spectrometer. In contrast, the laboratory rapidity is measured with respect to the direction of the proton beam and changes sign accordingly for the p–Pb and Pb–p configurations. In the semi-backward and semi-forward analyses, the negative rapidity points come from the Pb–p data, and the positive rapidity points from the p–Pb.

The ALICE apparatus consisted of 18 detector systems at the time the data used in this study were taken. The detectors relevant for the analysis are described in more detail below.

2.1 The ALICE central barrel

The innermost component of the central barrel is the Inner Tracking System (ITS) [22]. The ITS contains six cylindrical layers of silicon detectors, with the innermost layer at a radius of 3.9 cm with respect to the beam axis and the outermost layer at 43 cm. The two rings closest to the beam form the Silicon Pixel Detector (SPD) and cover the pseudorapidity ranges $|\eta| < 2$ and $|\eta| < 1.4$, for the inner and outer layers respectively. It is a fine granularity detector, having about 10^7 pixels. In addition to functioning as a tracking device, the SPD signals can be used to build triggers. The other four layers, two employing silicon drift chambers and two silicon microstrips, are used in this analysis exclusively for tracking.

The Time Projection Chamber (TPC), surrounding the ITS, is a large cylindrical detector used for tracking and for particle identification [23]. Its active volume extends from 85 to 247 cm in the radial direction and has a total length of 500 cm longitudinally, centred on the interaction point. A 100 kV central electrode separates its two drift volumes, providing an electric field for electron drift. The two end-plates are instrumented with Multi-Wire-Proportional-Chambers (MWPCs) with 560,000 readout pads in all, allowing high precision track measurements in the transverse plane. The z coordinate is given by the drift time in the TPC electric field. The TPC acceptance covers the pseudorapidity range $|\eta| < 0.9$ for tracks fully traversing it. Ionization measurements made along track clusters are used for particle identification.

Beyond the TPC lies the Time-of-Flight detector (TOF) [24]. It is a large cylindrical barrel of Multigap Resistive Plate Chambers (MRPCs) giving very high precision timing for tracks traversing it. Its pseudorapidity coverage matches that of the TPC. It is also capable of delivering signals for triggering purposes [25].

2.2 The ALICE muon spectrometer

The muon spectrometer consists of a 3 Tm dipole magnet, coupled with a tracking and a triggering system. A ten interaction-length conical front absorber, made of carbon, concrete and steel, is placed between the interaction point (IP) and the muon spectrometer tracking system, between 0.9 and 5 m from the IP, to filter out primary hadrons. Muon tracking is performed by means of five tracking stations, each one made of two planes of Cathode Pad Chambers. A 7.2 interaction-length iron wall is placed after the tracking stations. It is followed by the muon trigger system, based on two stations equipped with Resistive Plate Chambers. The trigger system can provide single-muon and dimuon triggers with a programmable p_T threshold. The p_T threshold is an approximate value owing to the coarse grain of the trigger spatial information. In addition, there is a conical absorber made of tungsten, lead and steel, that surrounds the beam

pipe at small angles ($\theta < 2^\circ$) and shields the spectrometer from secondary particles produced in interactions of primary particles in the beam pipe.

2.3 The V0 and the ZDC systems

Two sets of hadronic Zero Degree Calorimeters (ZDC) are located at 112.5 m on either side of the interaction point. Each station consists of two detectors, one to detect protons and the other neutrons. The neutron ZDCs detect neutrons emitted in the very forward region ($|\eta| > 8.7$). The calorimeters detect the Cherenkov light produced in quartz fibers by the hadronic showers. Each detector is read out by five photomultipliers. Their timing and energy resolution allow one to select events with neutrons produced at very forward rapidity, as could be the case in events with proton dissociation.

The V0 counters [26] consist of two arrays of 32 scintillator cells each, covering the range $2.8 < \eta < 5.1$ (V0A on the side opposite to the muon spectrometer) and $-3.7 < \eta < -1.7$ (V0C, on the same side as the muon spectrometer) and positioned respectively at $z = 340$ cm and $z = -90$ cm from the interaction point. The raw signals are used in the trigger, but are refined offline for use in the final data selections. For example, these detectors provide timing information with a resolution better than 1 ns, which can be used to distinguish two different timing windows, one corresponding to the passage of particles coming from collisions, and the other to particles coming from upstream interactions with residual gas molecules, termed “beam-gas” interactions.

2.4 Triggers

Two different signatures have been used in the analyses described below. In one case, the mid-rapidity analysis, the J/ψ candidate decays into a pair of leptons (either e^+e^- or $\mu^+\mu^-$), both of which are detected with the central barrel detectors. The second case, the semi-forward (or semi-backward) analysis, corresponds to a J/ψ candidate decaying into a pair of muons where one of them is measured with the muon spectrometer and the other with the central barrel detectors.

The trigger for the mid-rapidity analysis required at least two, and at most six, fired pad-OR in the TOF detector [24], such that at least two of the signals came from modules separated by more than 150 degrees in azimuth, since the J/ψ decay products are predominantly produced back-to-back in azimuth. The trigger also required no signal in V0A and no signal in V0C, to ensure that there is very little extra hadronic activity in the event, and at most six fired pixel chips in the outer layer of the SPD. In addition there were required to be two inner-outer pairs of these pixels having a back-to-back topology.

Three triggers were used for the semi-backward and semi-forward analyses. The first was active during the p–Pb data taking period. It required a muon candidate in the muon spectrometer trigger system with a transverse momentum above 0.5 GeV/c (as assessed in the trigger system electronics), at most 4 cells with signal in the V0C and no activity in the V0A. The SPD requirement was to have at least 1 pixel hit in either the inner or the outer layer and less than 7 pixels fired in the outer layer. Two different triggers were active during the Pb–p period. For the first one, in addition to the previous conditions, it was also required that at least one cell of the V0C had a signal. The second one had the same requirements as the first, but in addition vetoed signals from V0A compatible with beam-gas timing. These tighter conditions were required owing to an increased background trigger rate.

The integrated luminosity \mathcal{L}_{int} was corrected for the probability that the exclusivity requirements could be spoiled by multiple interactions in the same bunch crossing. This pile-up correction is on average 5%. The total luminosity of the sample used for the mid-rapidity analysis is 2.1 nb^{-1} (4.8 nb^{-1}) in the p–Pb (Pb–p) period, while for the semi-forward (semi-backward) analysis it is 3.1 nb^{-1} (3.7 nb^{-1}) in the p–Pb (Pb–p) period. Note that in the mid-rapidity case, the p–Pb and Pb–p data samples have been analysed together, taking into account the inversion of the rapidity sign, to increase the size of the central rapidity data sample.

3 Data samples

3.1 Event and track selection for the mid-rapidity analysis

The events used in the mid-rapidity analysis fulfilled the following criteria.

1. They fired the corresponding trigger.
2. There were exactly two tracks reconstructed with the TPC and the ITS.
3. The primary vertex had at least two tracks defining it.
4. Each track had at least 50 TPC space points out of a maximum of 159, a $\text{TPC-}\chi^2/\text{dof} < 4$, at least one SPD point and pseudorapidity $|\eta| < 0.9$.
5. The distance of closest approach of each track to the (nominal) primary vertex (DCA) was less than 2 cm in the longitudinal direction and less than $0.0182 + 0.035/p_T^{1.01}$ cm, with p_T in GeV/c, in the transverse direction [21].
6. Neither track was associated with a kink candidate.
7. The coordinate of the primary vertex of the interaction along the beam-line direction was within 15 cm of the nominal interaction point.
8. The two tracks had opposite electric charge.

To build dilepton candidates the tracks were separated into electrons and muons using the energy loss measured by the TPC, such that:

1. the quadratic sum of the normalised deviation from the corresponding Bethe-Bloch expectation for the positive and negative track had to be less than 16;
2. the rapidity, measured in the laboratory frame, of the dilepton candidate, formed by the 4-vector sum of the two tracks with the corresponding mass hypothesis, had to be in the range $|y| < 0.8$.

In addition, the events had to

3. have no signal in V0 as determined by the offline decision, and
4. no signal in either of the neutron ZDCs.

3.2 Event and track selection for the semi-backward and semi-forward analyses

The events used in the semi-backward and semi-forward analyses fulfilled the following criteria.

1. They fired the corresponding trigger.
2. There was exactly one track reconstructed with the TPC and the ITS.
3. This track fulfilled similar requirements to those for the central analysis tracks, with two modifications: it had to be compatible with a muon (within 4σ) according to the energy-loss measurement, and the acceptance was enlarged to $|\eta| < 1.1$.
4. Furthermore, the distance of closest approach of this track to the nominal interaction point had to be less than 15 cm in the direction along the beam-line.
5. The event also had to have exactly one track in the muon spectrometer such that:

- (a) the track is matched to a trigger track above the p_T threshold;
- (b) the radial coordinate of the track at the end of the front absorber (R_{abs}) was required to be in the range $17.5 \text{ cm} < R_{\text{abs}} < 89.5 \text{ cm}$;
- (c) it had a pseudorapidity in the range $-4.0 < \eta < -2.5$ ($-3.7 < \eta < -2.5$) in the p-Pb (Pb-p) period and fulfilled the so called $p \times \text{DCA}$ requirement.

The $p \times \text{DCA}$ requirement uses the difference in the distributions for signal and beam-induced background in the (p, DCA) plane, where p is the track momentum and DCA is the distance between the interaction vertex and the track extrapolated to the vertex transverse plane. If in a given event no interaction vertex was found, the point $(0, 0, 0)$ was used

to calculate the distance of closest approach. The pseudorapidity ranges are different in p-Pb and Pb-p owing to the additional V0C trigger requirement (see Sect. 2.4).

6. The two tracks had to have opposite electric charge.
7. The rapidity, measured in the laboratory frame, of the dimuon candidate, formed by the 4-vector sum of the two tracks with the muon-mass hypothesis, had to be in the range $1.2 < y < 2.7$ for the p-Pb and $-2.5 < y < -1.2$ for the Pb-p sample, respectively.
8. In addition, the events had to have no signal in V0A, at most one cell with a signal in V0C, (in both cases as determined by the offline reconstruction), no signal in either of the neutron ZDCs and at most one tracklet in the SPD layers.

3.3 Selection of background samples

Several background samples, one for each analysis, were selected. The events in these samples satisfy the conditions listed in the previous sections, and in addition there is required to be a signal, compatible with the presence of a neutron, in the ZDC placed in the proton direction. Both like-sign and opposite-sign dilepton candidates are accepted.

These samples are highly efficient to tag dissociative processes (where the target proton breaks up) and other hadronic collisions and were used to build templates to subtract the remaining background in the real data samples as explained below. As the trigger suppresses events with higher p_T dileptons ($p_T \geq 0.5 \text{ GeV}/c$), due to the condition on azimuthal separation, the number of events in this p_T range is limited. Therefore, each background spectrum was used to generate a high statistics sample, which was smoothed to produce the final template. This is referred to as “non-exclusive background” in the analysis of the p_T spectrum. The selections and smoothing algorithms were varied to estimate the systematic uncertainties, and the background p_T distribution was verified independently by selecting hadronic activity in V0C instead of the ZDC.

3.4 Monte Carlo samples

The STARLIGHT Monte Carlo generator [27,28] was used to generate large samples for the following processes: exclusive J/ψ photoproduction off proton ($\gamma p \rightarrow J/\psi p$) and Pb ($\gamma \text{Pb} \rightarrow J/\psi \text{Pb}$) targets, exclusive photoproduction of $\psi(2S)$ decaying into $J/\psi + X$, and continuum dilepton production $\gamma\gamma \rightarrow l^+l^-$. The physics models used by STARLIGHT are described in [28–30]. All generated events were passed through a full simulation of the detector based on GEANT 3 transport code [31] and subjected to the same analysis chain as real data. The Monte Carlo took into account

the changing status of the detectors during data-taking, and their residual misalignment.

In all cases the polarization of the photoproduced charmonium was taken as transverse, as expected for photoproduction of vector mesons. For the $\psi(2S)$ sample three cases were studied, corresponding to an assumption of longitudinal, transverse and no polarisation of the J/ψ produced by the decay of the $\psi(2S)$.

The dependence of exclusive photoproduction on the momentum transferred in the target vertex is modelled in STARLIGHT using an exponential distribution $F(Q^2) = e^{-bQ^2}$, with the slope b taking the default value of 4 GeV^{-2} [32]. HERA measurements have shown that the value of this parameter depends on $W_{\gamma p}$ [10]. This effect is particularly important for the mid-rapidity and the semi-backward samples, where $W_{\gamma p}$ is larger. To take this into account additional samples of exclusive J/ψ were produced using STARLIGHT with a value of b given by the H1 parameterisation from [10].

4 Data analysis

4.1 Signal extraction

The mass distributions for the dilepton candidates that passed the selection described in the previous section are shown in Fig. 1. In all cases a clear J/ψ signal is observed over a small background. The data can be satisfactorily described in all cases by a combination of a Crystal-Ball function (CB) [33] and an exponential distribution, which represent the signal and the background from continuum dilepton production, respectively. The tail parameters of the CB distribution have been fixed to the values obtained by fitting simulated events.

Figure 2 shows the distribution of transverse momentum for dilepton pairs having mass (m_{l+l-}) in the range $2.9 < m_{l+l-} < 3.2 \text{ GeV}/c^2$ for all the samples, except for the dimuon case in the mid-rapidity analysis where the lower bound was raised to $3.0 \text{ GeV}/c^2$ to make use of the better mass resolution of this channel. In all cases the transverse momenta populate the region below about $1 \text{ GeV}/c$, as expected from exclusive photoproduction off protons. These distributions are used to extract the number of exclusive J/ψ , within the stipulated mass range, in each of the measured rapidity intervals. An extended binned likelihood method is used in fits of data to a sum of templates for signal and background obtained from data (see Sect. 3.3) and from Monte Carlo (see Sect. 3.4) samples. These templates are also shown in the figure.

The number of candidates from the continuum dilepton template, which is a free parameter in the fit, was found always to be less than what is obtained, in the given mass range, from the exponential part of the fit to the mass distribution. This exponential distribution includes both the exclu-

sive and the dissociative dilepton production, while the template describes only the exclusive component. The number of candidates for coherent J/ψ production off lead has been estimated using STARLIGHT. The STARLIGHT predictions were rescaled so as to be compatible, within the uncertainties, with ALICE measurements in Pb–Pb collisions [34, 35]. The normalisation of the exclusive J/ψ and non-exclusive background templates have been left free. Note that the non-exclusive background is lower at higher energies of the photon-target system, as has already been observed at HERA [10, 11], and also by ALICE [19].

The number of candidates obtained from the fitted template for exclusive J/ψ production has been corrected for the feed-down from exclusive production of $\psi(2S)$ decaying into $J/\psi + X$ [35]. This correction amounts to about 2% (4%) for the semi-backward and semi-forward (mid-rapidity) analyses. The correction factor to take into account the acceptance and efficiency ($\varepsilon \times A$) of the detector was computed using simulated events, as described in Sect. 3.4. This factor depends on the rapidity of the J/ψ and varies from around 3% to almost 9%. For the semi-backward sample the $\varepsilon \times A$ includes the efficiency of the V0C (around 60%) to detect the passing muon (because it is included in the trigger). The values for the number of exclusive J/ψ extracted in the different data samples, as well as the corresponding $\varepsilon \times A$ factors and available luminosity, are summarised in Table 1. Note that, in order to make best use of the available statistics, both the central and the semi-forward (but not the semi-backward) samples have been sub-divided into two rapidity bins.

4.2 Estimation of systematic uncertainties

Several sources of systematic uncertainty have been studied. They are discussed below, while their contribution to the uncertainty on the measured cross sections are summarised in Table 2.

The uncertainty on the tracking efficiency in the TPC was estimated repeating the analyses using different track selections. Four different values for the minimal number of points and three values for the minimum number of TPC pads crossed by the track were used. The systematic uncertainty related to the selection of tracks at mid-rapidity was estimated from the spread of the variations with respect to the standard selection. It varies from 0.8 to 5.7%.

The uncertainty related to the identification of electrons and muons using their energy deposition in TPC has been obtained using an alternative selection based directly on the energy loss [36]. The difference between the two methods was used as an estimate of the systematic uncertainty, and was at most 1.3%. Cross contamination from muon pairs in the electron sample and vice versa was found to be negligible.

The uncertainty on the single muon tracking efficiency in the muon spectrometer was obtained by comparing the results

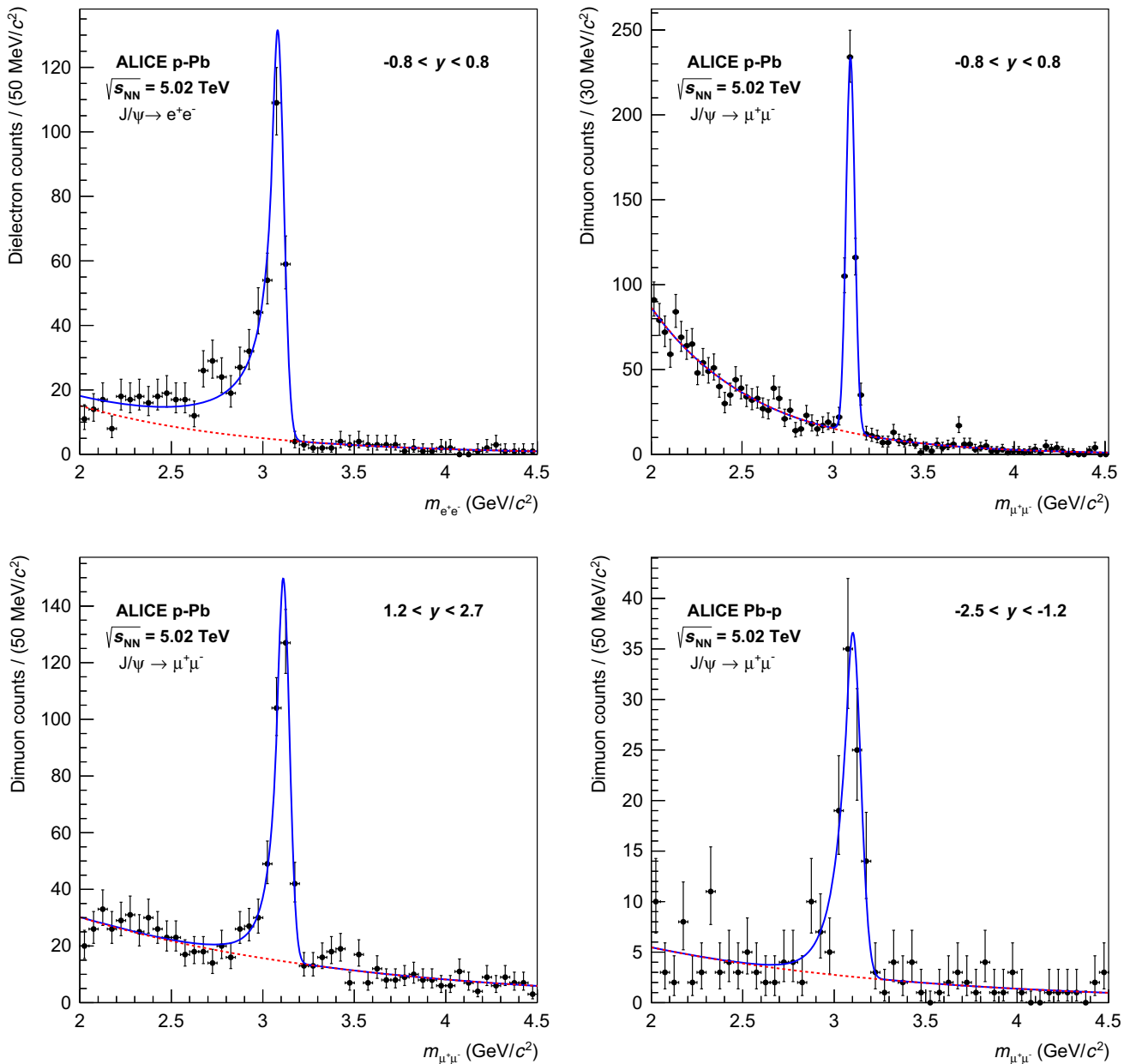


Fig. 1 Mass distributions of selected dileptons for the dielectron (upper left) and dimuon (upper right) samples for the central analysis and dimuon samples for the semi-forward (lower left) and semi-backward (lower right) analyses. In all cases the data are represented

by points with error bars. The solid blue line is a fit to a Crystal-Ball function plus an exponential distribution, where this last contribution is shown by a dotted red line

of measurements performed on simulations with those from real data [35] and amounts to 2% (3%) for the p–Pb (Pb–p) period. There is also a 0.5% contribution from variations on the conditions required to match the trigger and the tracking information of a given muon.

The uncertainties related to triggering in the muon spectrometer have been evaluated as in [36]. The efficiency maps of the trigger chambers have been obtained using data. The statistical uncertainty on this procedure has been used to vary

the efficiency in simulations, which was then used to estimate a systematic uncertainty of 1%. There is also a small discrepancy between the efficiency in data and in simulations around the trigger threshold. This gives a contribution of 1.7% (1.3%) for the p–Pb (Pb–p) period. The addition in quadrature of these two effects yields the uncertainty on muon triggering.

The two main contributions to the uncertainty on the trigger efficiency for the mid-rapidity analysis come from

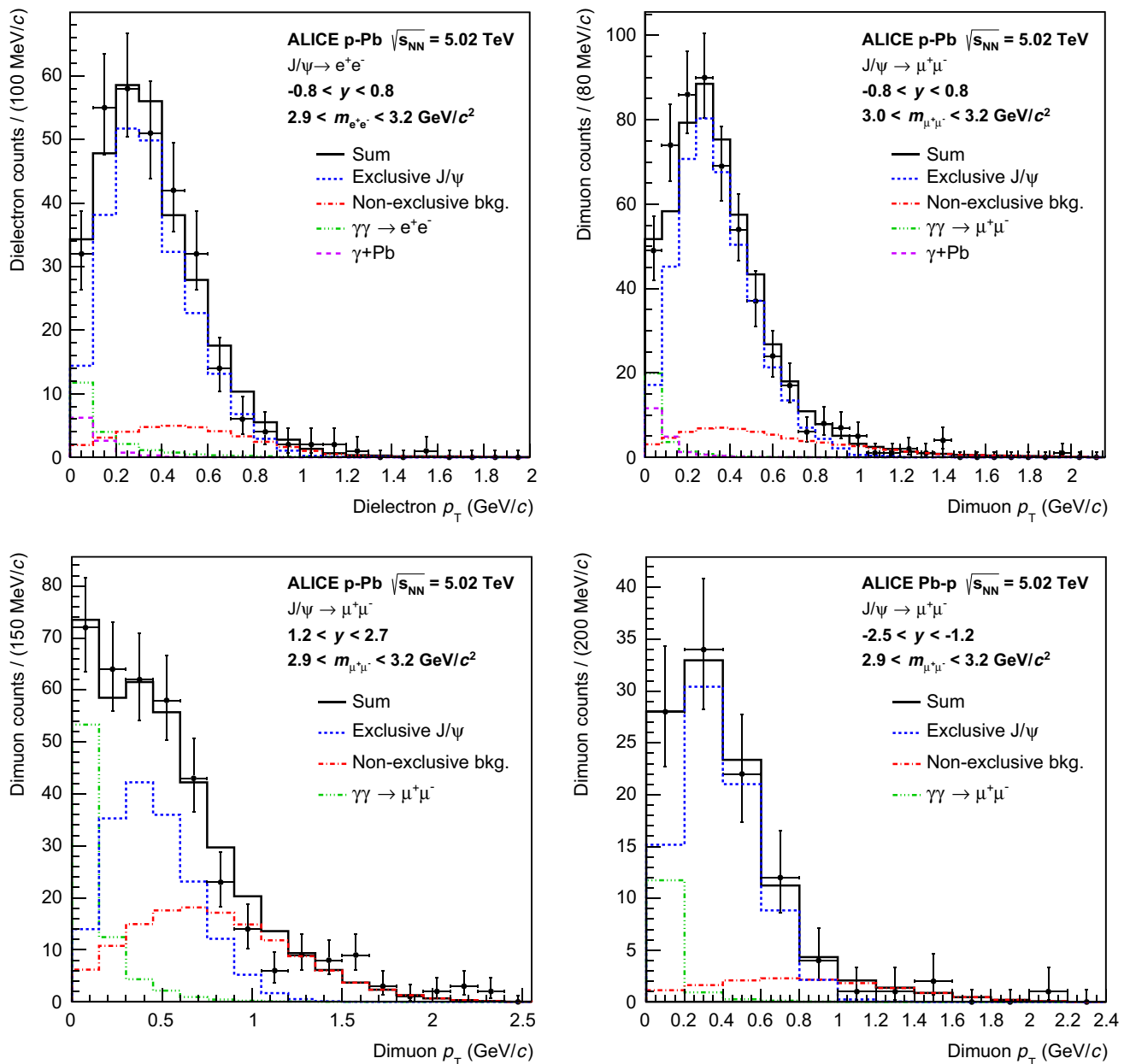


Fig. 2 Transverse momentum distributions of dileptons around the J/ψ mass for the dielectron (upper left) and dimuon (upper right) samples for the central analysis and dimuon samples for the semi-forward (lower left) and semi-backward (lower right) analyses. In all cases the data are represented by points with error bars. The blue, magenta (dash)

and green (dash-dot-dot) lines correspond to Monte Carlo templates for J/ψ coming from exclusive photoproduction off protons or off lead and continuous dilepton production respectively. The red (dash-dot) line is a template for dissociative and hadronic background obtained from data. The solid black line is the sum of all contributions

the back-to-back topology condition in the SPD and TOF detectors. The first one was estimated using a data sample obtained using a zero-bias trigger (all bunch crossings taken). It amounts to 4.5%. The second one was taken from the analysis of [35]. It amounts to $(-9\%, +3.8\%)$, using a zero bias trigger to compute the efficiency and comparing the result with the efficiency from simulated events.

The efficiency of the V0C to detect one muon from the J/ψ decay, which is needed in the semi-backward analysis, was estimated using events from the p–Pb period, whose trigger did not include this V0C requirement. The procedure was cross checked using the forward dimuon sample used for the analysis described in [19]. The efficiency depends slightly on the mass range used to compute it. The addition in quadrature of the statistical uncertainty (2.7%) and

Table 1 Number of measured exclusive J/ψ , value of the efficiency and acceptance correction factor, as well as integrated luminosity for each rapidity interval. These values are used in Eq. (1) to compute the measured cross sections

Rapidity	$N_{J/\psi}$	$\varepsilon \times A$	\mathcal{L}_{int} (nb^{-1})
(1.9, 2.7)	73 ± 15	0.071	3.147
(1.2, 1.9)	98 ± 17	0.086	3.147
(0.0, 0.8)			
Dielectron	106 ± 16	0.029	6.915
Dimuon	196 ± 17	0.057	6.915
(−0.8, 0.0)			
Dielectron	117 ± 13	0.033	6.915
Dimuon	199 ± 20	0.063	6.915
(−2.5, −1.2)	76 ± 11	0.037	3.743

the mass dependence (2.0%) yields an uncertainty of 3.4%. The veto efficiency of the V0 detector can also be estimated offline using a more complex algorithm than that used in the online trigger. To estimate the uncertainty on the use of V0 to veto extra activity, the analyses were compared using the online V0 decision only and requiring (standard selection) in addition the offline decision, with the difference giving the systematic uncertainty. The uncertainty varies from 1.2% to 3.5%.

The trigger conditions associated with the upper limits in the activity in TOF, SPD and V0C have a negligible effect on the systematic uncertainty, because the limits are set well above the levels of activity produced by the signal in our sample.

The systematic uncertainty on the yield was obtained by varying the range of fit to the transverse momentum template, the width of the binning and the selections and smoothing

algorithms used to determine the non-exclusive template (see Sect. 3.3). Furthermore, the value of the b parameter used in the production of the exclusive J/ψ template was varied, taking into account the uncertainties reported by H1 [10]. The uncertainty varies from 1.9 to 3.6% (see “signal extraction” in Table 2).

The polarization of the J/ψ coming from $\psi(2S)$ feed-down is not known. The uncertainty on the amount of feed-down has been estimated by assuming that the J/ψ was either not polarised or that it was fully transversely or fully longitudinally polarised. This uncertainty is asymmetric and varies from +1.0 to −1.4% (see “feed-down” in Table 2).

The uncertainty on the measurement of the luminosity has a contribution of 1.6%, which is correlated between the p–Pb and Pb–p data-taking periods and, in addition, an uncorrelated part of 3.3% (3.0%) in the p–Pb (Pb–p) configuration [37]. For the mid-rapidity analysis, which has data from both p–Pb and Pb–p, the uncorrelated part of the uncertainty on the luminosity amounts to 2.3%.

Furthermore, the uncertainties on the TPC selection, particle identification, offline V0 veto efficiency and signal extraction are uncorrelated across rapidity. The uncertainty on the $\psi(2S)$ feed-down is correlated for all rapidities. The uncertainties on muon tracking, matching and trigger efficiencies are mostly uncorrelated across rapidity, and for the purposes of this analysis we treat the uncertainties as fully uncorrelated. (This includes also the measurements from [19].) The trigger efficiency at mid-rapidity is correlated between the (0.0,0.8) and (−0.8,0.0) rapidity intervals.

The mid-rapidity analysis offers two other possibilities to cross check the consistency of the results. One can compare the results of the cross section in the p–Pb and Pb–p periods, and one can compare the results of the electron and the muon decay channels. The cross sections agreed in all cases

Table 2 Summary of the contributions to the systematic uncertainty, in percent, for the J/ψ cross section in the different rapidity intervals

	(1.9, 2.7)	(1.2, 1.9)	(0.0, 0.8)	(−0.8, 0.0)	(−2.5, −1.2)
TPC track selection	5.7	1.2	0.9	0.8	3.3
Particle identification	–	–	1.3	0.6	–
Muon tracking efficiency	2.0	2.0	–	–	3.0
Muon matching efficiency	0.5	0.5	–	–	0.5
Trigger efficiency	2.0	2.0	$^{+5.9}_{-10.1}$	$^{+5.9}_{-10.1}$	1.6
V0C Trigger efficiency	–	–	–	–	3.4
Offline V0 veto efficiency	2.7	3.5	2.1	2.1	1.2
Signal extraction	3.6	2.2	2.1	1.9	3.0
Feed-down	$^{+0.0}_{-1.3}$	1.0	$^{+0.6}_{-1.0}$	$^{+1.0}_{-0.6}$	$^{+0.0}_{-1.4}$
Luminosity uncorrelated	3.3	3.3	2.3	2.3	3.0
Luminosity correlated	1.6	1.6	1.6	1.6	1.6
Branching ratio [38]	0.6	0.6	0.4	0.4	0.6
Total	8.7	6.4	11.1	11.0	7.7

Table 3 Measured differential cross sections $d\sigma/dy$ for exclusive J/ψ photoproduction off protons in ultra-peripheral p–Pb (positive rapidity values) and Pb–p (negative rapidity values) collisions at $\sqrt{s_{NN}} = 5.02$ TeV in the different rapidity intervals. Values of the photon flux $k dn/dk$, the interval in $W_{\gamma p}$ corresponding to the rapidity, the average $W_{\gamma p}$

($\langle W_{\gamma p} \rangle$) and the extracted cross section $\sigma(\gamma + p \rightarrow J/\psi + p)$. The first uncertainty in the cross sections is statistical, the second is systematic and the third comes from the uncertainty in the photon flux

Rapidity	$\frac{d\sigma}{dy}$ (μb)	$k \frac{dn}{dk}$	$W_{\gamma p}$ (GeV)	$\langle W_{\gamma p} \rangle$ (GeV)	$\sigma(\gamma + p \rightarrow J/\psi + p)$ (nb)
(1.9, 2.7)	$6.9 \pm 1.4 \pm 0.6$	163.6 ± 1.5	(40.8, 60.9)	50.4	$42 \pm 9 \pm 4 \pm 1$
(1.2, 1.9)	$8.7 \pm 1.5 \pm 0.6$	140.2 ± 1.5	(60.9, 86.4)	73.1	$62 \pm 11 \pm 4 \pm 1$
(0.0, 0.8)	$10.6 \pm 0.8 \pm 1.2$	104.3 ± 1.5	(105.5, 157.4)	129.9	$101 \pm 8 \pm 11 \pm 1$
(− 0.8, 0.0)	$10.0 \pm 0.8 \pm 1.1$	79.4 ± 1.5	(157.4, 234.9)	193.3	$126 \pm 10 \pm 14 \pm 2$
(− 2.5, − 1.2)	$7.1 \pm 1.0 \pm 0.5$	36.5 ± 1.4	(286.9, 549.5)	391.2	$194 \pm 27 \pm 15 \pm 7$

within the statistical uncertainties. As a cross-check, the possible contribution from incoherent production of J/ψ off the Pb nucleus was investigated, and found to be negligible. In addition, the effect on the $\varepsilon \times A$ correction of varying the slope parameter b within the HERA limits was also found to be negligible.

Systematic effects related to noise or pileup events in the ZDC are estimated using randomly triggered events and are also found to be negligible.

5 Results

5.1 Cross sections for exclusive production of J/ψ in p–Pb collisions

The measured cross section for the exclusive production of J/ψ in collisions of protons with lead nuclei is computed according to

$$\frac{d\sigma}{dy} = \frac{N_{J/\psi}}{\varepsilon \times A \cdot \text{BR}(J/\psi \rightarrow l^+l^-) \cdot \mathcal{L}_{\text{int}} \cdot \Delta y} \quad (1)$$

where Δy represents the width of the rapidity region where the measurement is performed and the branching ratios are $\text{BR}(J/\psi \rightarrow e^+e^-) = (5.97 \pm 0.03)\%$ and $\text{BR}(J/\psi \rightarrow \mu^+\mu^-) = (5.96 \pm 0.03)\%$ according to [38]. The values that go into this equation are listed in Table 1, while the measured cross sections are given in Table 3.

For the mid-rapidity analysis the measurements in the muon and electron channels are computed independently. The cross sections in the rapidity range $-0.8 < y < 0$ ($0 < y < 0.8$) are 10.7 ± 1.3 (11.1 ± 1.8) μb for the electron channel and 9.6 ± 1.0 (10.4 ± 1.0) μb for the muon channel, where the errors represent the statistical uncertainty. These measurements have been averaged, weighting each cross section with its statistical uncertainty.

5.2 Cross sections for exclusive photoproduction of J/ψ off protons

The relation between $d\sigma/dy$ and the cross section for the photoproduction of J/ψ off protons, $\sigma(\gamma + p \rightarrow J/\psi + p)$, is given by

$$\frac{d\sigma}{dy} = k \frac{dn}{dk} \sigma(\gamma + p \rightarrow J/\psi + p) \quad (2)$$

where $k = 0.5 \times M_{J/\psi} \exp(-y)$ is the photon energy in the laboratory frame and $k dn/dk$ the flux of photons with energy k emitted by the lead nucleus. Using STARLIGHT, the flux has been computed in impact parameter space and convoluted with the probability of no hadronic interaction. The uncertainty in the flux is obtained varying the radius of the lead nucleus, used in the nuclear form factor, by ± 0.5 fm, which corresponds to the nuclear skin thickness.

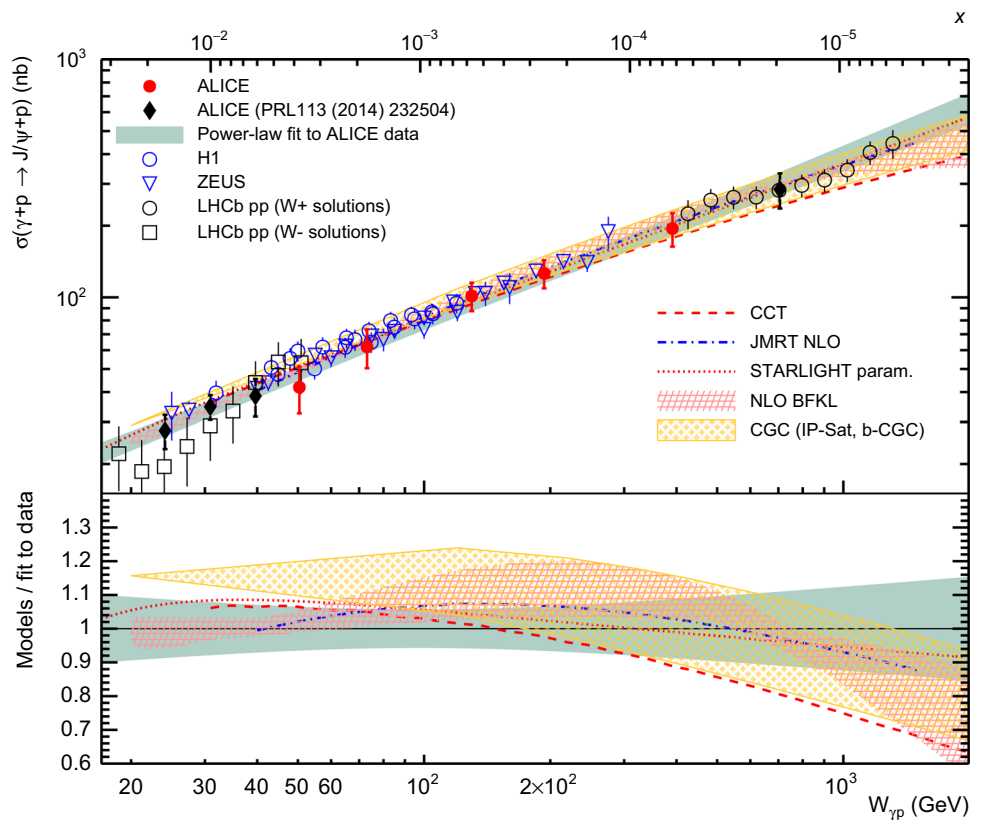
The measured cross sections are given in Table 3, and also include the value of the centre-of mass energy of the photon-proton system, $\langle W_{\gamma p} \rangle$, computed as the average of $W_{\gamma p}$ over the rapidity interval weighted by the photoproduction cross section predicted by STARLIGHT.

5.3 Energy dependence of the exclusive photoproduction of J/ψ off protons

Figure 3 shows all ALICE measurements, including those from [19], for the exclusive photoproduction of J/ψ off protons as a function of $W_{\gamma p}$. The data cover the $W_{\gamma p}$ range from 24 to 706 GeV, which corresponds roughly to three orders of magnitude in x , from $\sim 2 \times 10^{-2}$ to $\sim 2 \times 10^{-5}$. The error bars are the quadratic sum of the statistical and the total systematic uncertainties.

The same figure shows the result of a χ^2 -fit of a power law $N(W_{\gamma p}/W_0)^\delta$ to the full set of ALICE data, with $W_0 = 90.0$ GeV as was done before in HERA analyses [40]. The fit takes into account the statistical and systematic uncertainties, according to the technique used by H1 in [41]. The parameters found by the fit are $N = 71.8 \pm 4.1$ nb and

Fig. 3 (Upper panel) ALICE data (red symbols) on exclusive photoproduction of J/ψ off protons as a function of the centre-of-mass energy of the photon–proton system $W_{\gamma p}$, obtained in collisions of protons and lead nuclei at $\sqrt{s_{NN}} = 5.02$ TeV, including results from [19], compared to a power-law fit, to data from HERA [9, 11], to the solutions from LHCb [39] and to theoretical models (see text). The uncertainties are the quadratic sum of the statistical and systematic uncertainties. (Lower panel) Ratio of the models shown in the upper panel to the power law fit through the ALICE data points. The Bjorken x value corresponding to $W_{\gamma p}$ is also displayed on the top of the figure, see text for details



$\delta = 0.70 \pm 0.05$ with a correlation of -0.06 between both parameters. The quality of the fit is $\chi^2 = 1.21$ for 7 degrees of freedom. The value of the exponent is compatible to that found using previous ALICE data [19], as well as with that found by HERA experiments [9, 11].

The comparison of ALICE measurements to data from other experiments as well as to the results from different models is also shown in Fig. 3. HERA [9, 11] and ALICE data are compatible within uncertainties. LHCb measured the exclusive production of J/ψ in pp collisions, where the photon source can not be identified. Thus the extraction of the photoproduction cross section is not possible without further assumptions. For each measurement they reported two solutions [14] which also agree with ALICE measurements.

ALICE measurements are also compared to theory in Fig. 3. The JMRT group [42] has two computations, one is based on the leading-order (LO) result from [8] with the addition of some corrections to the cross section, while the second includes also the main contributions expected from a next-to-leading order (NLO) result. The parameters of both models have been obtained by a fit to the same data and their energy dependence is rather similar, so only the NLO version is shown. Recently, three new studies have appeared, describing the $W(\gamma p)$ dependence of the exclusive J/ψ cross section in terms of a colour dipole model [43] (CGC) or of the BFKL evolution of HERA values (HERA Fit 2) with a photopro-

duction scale $M^2 = 2.39 \text{ GeV}^2$ [44] (NLO(BFKL)). These are shown as bands in the figure. A third model, based on the colour dipole approach, and incorporating the energy dependence of geometrical fluctuations of the proton structure in the impact parameter plane [45] is also shown (CCT). The models are in reasonable agreement with our data. Finally the STARLIGHT parameterisation relies on a power-law fit to fixed-target and HERA data. This model also agrees with our measurement.

6 Summary

The ALICE Collaboration has measured the photoproduction of J/ψ mesons off protons in p–Pb interactions. New measurements, summarised in Table 3, at central, semi-backward and semi-forward rapidities are added to those previously given at forward and backward rapidities. Each rapidity interval corresponds to a given energy for exclusive photoproduction in photon–proton interactions. The data agree with the previous ALICE measurements at forward and backward rapidities, with the LHCb results in pp interactions and with previous HERA measurements over a smaller energy range. The ALICE measurements are consistent with a power law dependence $\sigma(\gamma p \rightarrow J/\psi p) \sim W_{\gamma p}^\delta$, with $\delta = 0.70 \pm 0.05$. Several models, based on different physics assumptions,

reproduced this behaviour within the current experimental uncertainties. The model predictions around and above 1 TeV are not very precise although all tend to go below the extrapolation of the fit, as shown in the lower panel of Fig. 3. This energy range will be reachable with the new LHC data from Run 2 and the data to be collected in Run 3 and Run 4. The data presented here, augmented with the results from future measurements, will be a powerful tool to better understand the role of saturation at the highest energies.

Acknowledgements The ALICE Collaboration would like to thank all its engineers and technicians for their invaluable contributions to the construction of the experiment and the CERN accelerator teams for the outstanding performance of the LHC complex. The ALICE Collaboration gratefully acknowledges the resources and support provided by all Grid centres and the Worldwide LHC Computing Grid (WLCG) collaboration. The ALICE Collaboration acknowledges the following funding agencies for their support in building and running the ALICE detector: A. I. Alikhanyan National Science Laboratory (Yerevan Physics Institute) Foundation (ANSL), State Committee of Science and World Federation of Scientists (WFS), Armenia; Austrian Academy of Sciences and Nationalstiftung für Forschung, Technologie und Entwicklung, Austria; Ministry of Communications and High Technologies, National Nuclear Research Center, Azerbaijan; Conselho Nacional de Desenvolvimento Científico e Tecnológico (CNPq), Universidade Federal do Rio Grande do Sul (UFRGS), Financiadora de Estudos e Projetos (Finep) and Fundação de Amparo à Pesquisa do Estado de São Paulo (FAPESP), Brazil; Ministry of Science & Technology of China (MSTC), National Natural Science Foundation of China (NSFC) and Ministry of Education of China (MOEC), China; Ministry of Science and Education, Croatia; Centro de Aplicaciones Tecnológicas y Desarrollo Nuclear (CEADEN), Cubaenergía, Cuba; Ministry of Education, Youth and Sports of the Czech Republic, Czech Republic; The Danish Council for Independent Research | Natural Sciences, the Carlsberg Foundation and Danish National Research Foundation (DNRF), Denmark; Helsinki Institute of Physics (HIP), Finland; Commissariat à l’Energie Atomique (CEA) and Institut National de Physique Nucléaire et de Physique des Particules (IN2P3) and Centre National de la Recherche Scientifique (CNRS), France; Bundesministerium für Bildung, Wissenschaft, Forschung und Technologie (BMBF) and GSI Helmholtzzentrum für Schwerionenforschung GmbH, Germany; General Secretariat for Research and Technology, Ministry of Education, Research and Religions, Greece; National Research, Development and Innovation Office, Hungary; Department of Atomic Energy Government of India (DAE), Department of Science and Technology, Government of India (DST), University Grants Commission, Government of India (UGC) and Council of Scientific and Industrial Research (CSIR), India; Indonesian Institute of Science, Indonesia; Centro Fermi - Museo Storico della Fisica e Centro Studi e Ricerche Enrico Fermi and Istituto Nazionale di Fisica Nucleare (INFN), Italy; Institute for Innovative Science and Technology, Nagasaki Institute of Applied Science (IIST), Japan Society for the Promotion of Science (JSPS) KAKENHI and Japanese Ministry of Education, Culture, Sports, Science and Technology (MEXT), Japan; Consejo Nacional de Ciencia (CONACYT) y Tecnología, through Fondo de Cooperación Internacional en Ciencia y Tecnología (FONCICYT) and Dirección General de Asuntos del Personal Académico (DGAPA), Mexico; Nederlandse Organisatie voor Wetenschappelijk Onderzoek (NWO), Netherlands; The Research Council of Norway, Norway; Commission on Science and Technology for Sustainable Development in the South (COMSATS), Pakistan; Pontificia Universidad Católica del Perú, Peru; Ministry of Science and Higher Education and National Science Centre, Poland; Korea Institute of Science and Technology Information and National Research Foundation

of Korea (NRF), Republic of Korea; Ministry of Education and Scientific Research, Institute of Atomic Physics and Romanian National Agency for Science, Technology and Innovation, Romania; Joint Institute for Nuclear Research (JINR), Ministry of Education and Science of the Russian Federation and National Research Centre Kurchatov Institute, Russia; Ministry of Education, Science, Research and Sport of the Slovak Republic, Slovakia; National Research Foundation of South Africa, South Africa; Swedish Research Council (VR) and Knut & Alice Wallenberg Foundation (KAW), Sweden; European Organization for Nuclear Research, Switzerland; National Science and Technology Development Agency (NSDTA), Suranaree University of Technology (SUT) and Office of the Higher Education Commission under NRU project of Thailand, Thailand; Turkish Atomic Energy Agency (TAEK), Turkey; National Academy of Sciences of Ukraine, Ukraine; Science and Technology Facilities Council (STFC), United Kingdom; National Science Foundation of the United States of America (NSF) and United States Department of Energy, Office of Nuclear Physics (DOE NP), United States of America.

Data Availability Statement This manuscript has associated data in a data repository. [Authors’ comment: The numerical values of the data points will be uploaded to HEPData.]

Open Access This article is distributed under the terms of the Creative Commons Attribution 4.0 International License (<http://creativecommons.org/licenses/by/4.0/>), which permits unrestricted use, distribution, and reproduction in any medium, provided you give appropriate credit to the original author(s) and the source, provide a link to the Creative Commons license, and indicate if changes were made. Funded by SCOAP³.

References

1. F. Gelis, E. Iancu, J. Jalilian-Marian, R. Venugopalan, The color glass condensate. *Ann. Rev. Nucl. Part. Sci.* **60**, 463–489 (2010). [arXiv:1002.0333](https://arxiv.org/abs/1002.0333) [hep-ph]
2. ZEUS, H1 Collaboration, F. D. Aaron et al., Combined measurement and QCD analysis of the inclusive $e^{\pm} p$ scattering cross sections at HERA. *JHEP* **01**, 109 (2010). [arXiv:0911.0884](https://arxiv.org/abs/0911.0884) [hep-ex]
3. ZEUS, H1 Collaboration, H. Abramowicz et al., Combination of measurements of inclusive deep inelastic $e^{\pm} p$ scattering cross sections and QCD analysis of HERA data. *Eur. Phys. J. C* **75**(12), 580 (2015). [arXiv:1506.06042](https://arxiv.org/abs/1506.06042) [hep-ex]
4. L. Gribov, E. Levin, M. Ryskin, Semihard processes in QCD. *Phys. Rept.* **100**, 1–150 (1983)
5. A.H. Mueller, Small x behavior and parton saturation: a QCD model. *Nucl. Phys. B* **335**, 115 (1990)
6. LHeC Study Group Collaboration, J. L. Abelleira Fernandez et al., A large Hadron electron collider at CERN: report on the physics and design concepts for machine and detector. *J. Phys. G* **39**, 075001 (2012). [arXiv:1206.2913](https://arxiv.org/abs/1206.2913) [physics.acc-ph]
7. A. Accardi et al., Electron ion collider: the next QCD frontier. *Eur. Phys. J. A* **52**(9), 268 (2016). [arXiv:1212.1701](https://arxiv.org/abs/1212.1701) [nucl-ex]
8. M. Ryskin, Diffractive J/ψ electroproduction in LLA QCD. *Z. Phys. C* **57**, 89–92 (1993)
9. ZEUS Collaboration, S. Chekanov et al., Exclusive photoproduction of J/ψ mesons at HERA. *Eur. Phys. J. C* **24**, 345–360 (2002). [arXiv:hep-ex/0201043](https://arxiv.org/abs/hep-ex/0201043) [hep-ex]
10. H1 Collaboration, A. Aktas et al., Elastic J/ψ production at HERA. *Eur. Phys. J. C* **46**, 585–603 (2006). [arXiv:hep-ex/0510016](https://arxiv.org/abs/hep-ex/0510016) [hep-ex]
11. H1 Collaboration, C. Alexa et al., Elastic and proton-dissociative photoproduction of J/ψ mesons at HERA. *Eur. Phys. J. C* **73**, 2466 (2013). [arXiv:1304.5162](https://arxiv.org/abs/1304.5162) [hep-ex]

12. H1 Collaboration, C. Adloff et al., Diffractive photoproduction of $\psi(2S)$ mesons at HERA. *Phys. Lett. B* **541**, 251–264 (2002). [arXiv:hep-ex/0205107](#) [hep-ex]
13. CDF Collaboration, T. Aaltonen et al., Observation of exclusive charmonium production and $\gamma + \gamma$ to $\mu^+\mu^-$ in $p\bar{p}$ collisions at $\sqrt{s} = 1.96$ TeV. *Phys. Rev. Lett.* **102**, 242001 (2009). [arXiv:0902.1271](#) [hep-ex]
14. LHCb Collaboration, R. Aaij et al., Updated measurements of exclusive J/ψ and $\psi(2S)$ production cross-sections in pp collisions at $\sqrt{s} = 7$ TeV. *J. Phys. G* **41**, 055002. [arXiv:1401.3288](#) [hep-ex]
15. H1 Collaboration, C. Adloff et al., Elastic photoproduction of J/ψ and Υ mesons at HERA. *Phys. Lett. B* **483**, 23–35 (2000). [arXiv:hep-ex/0003020](#) [hep-ex]
16. Z.E.U.S. Collaboration, S. Chekanov et al., Exclusive photoproduction of Υ mesons at HERA. *Phys. Lett. B* **680**, 4–12 (2009). [arXiv:0903.4205](#) [hep-ex]
17. Z.E.U.S. Collaboration, H. Abramowicz et al., Measurement of the t dependence in exclusive photoproduction of $\Upsilon(1S)$ mesons at HERA. *Phys. Lett. B* **708**, 14–20 (2012). [arXiv:1111.2133](#) [hep-ex]
18. LHCb Collaboration, R. Aaij et al., Measurement of the exclusive J/ψ production cross-section in pp collisions at $\sqrt{s} = 7$ TeV and 8 TeV. *JHEP* **09**, 084 (2015). [arXiv:1505.08139](#) [hep-ex]
19. ALICE Collaboration, B.B. Abelev et al., Exclusive J/ψ photoproduction off protons in ultra-peripheral p–Pb collisions at $\sqrt{s_{NN}} = 5.02$ TeV. *Phys. Rev. Lett.* **113**(23), 232504 (2014). [arXiv:1406.7819](#) [nucl-ex]
20. ALICE Collaboration, K. Aamodt et al., The ALICE experiment at the CERN LHC. *JINST* **3**, S08002 (2008)
21. ALICE Collaboration, B.B. Abelev et al., Performance of the ALICE Experiment at the CERN LHC. *Int. J. Mod. Phys. A* **29**, 1430044 (2014). [arXiv:1402.4476](#) [nucl-ex]
22. ALICE Collaboration, K. Aamodt et al., Alignment of the ALICE inner tracking system with cosmic-ray tracks. *JINST* **5**, P03003 (2010). [arXiv:1001.0502](#) [physics.ins-det]
23. J. Alme et al., The ALICE TPC, a large 3-dimensional tracking device with fast readout for ultra-high multiplicity events. *Nucl. Instrum. Meth. A* **622**, 316–367 (2010). [arXiv:1001.1950](#) [physics.ins-det]
24. A. Akindinov et al., Performance of the ALICE time-of-flight detector at the LHC. *Eur. Phys. J. Plus* **128**, 44 (2013)
25. A. Akindinov et al., A topological trigger based on the time-of-flight detector for the alice experiment. *Nuclear instruments and methods in physics research section A: accelerators, spectrometers, detectors and associated equipment.* **602**(2), 372–376 (2009). <http://www.sciencedirect.com/science/article/pii/S0168900208018093>
26. ALICE Collaboration, E. Abbas et al., Performance of the ALICE VZERO system. *JINST* **8**, P10016 (2013). [arXiv:1306.3130](#) [nucl-ex]
27. STARLIGHT website. <http://starlight.hepforge.org/>
28. S.R. Klein, J. Nystrand, J. Seger, Y. Gorbunov, J. Butterworth, STARlight: a Monte Carlo simulation program for ultra-peripheral collisions of relativistic ions. *Comput. Phys. Commun.* **212**, 258–268 (2017). [arXiv:1607.03838](#) [hep-ph]
29. S. Klein, J. Nystrand, Exclusive vector meson production in relativistic heavy ion collisions. *Phys. Rev. C* **60**, 014903 (1999). [arXiv:hep-ph/9902259](#) [hep-ph]
30. A.J. Baltz, Y. Gorbunov, S.R. Klein, J. Nystrand, Two-photon interactions with nuclear breakup in relativistic heavy ion collisions. *Phys. Rev. C* **80**, 044902 (2009). [arXiv:0907.1214](#) [nucl-ex]
31. R. Brun, F. Bruyant, M. Maire, A.C. McPherson, and P. Zanzarini, “GEANT3;”. CERN-DD-EE-84-1
32. S.R. Klein, J. Nystrand, Interference in exclusive vector meson production in heavy-ion collisions. *Phys. Rev. Lett.* **84**, 2330–2333 (2000). <https://doi.org/10.1103/PhysRevLett.84.2330>
33. T. Skwarnicki, A study of the radiative cascade transitions between the upsilon-prime and upsilon resonances. DESY-F31-86-02
34. ALICE Collaboration, B. Abelev et al., Coherent J/ψ photoproduction in ultra-peripheral Pb–Pb collisions at $\sqrt{s_{NN}} = 2.76$ TeV. *Phys. Lett. B* **718**, 1273–1283 (2013). [arXiv:1209.3715](#) [nucl-ex]
35. ALICE Collaboration, E. Abbas et al., Charmonium and e^+e^- pair photoproduction at mid-rapidity in ultra-peripheral Pb–Pb collisions at $\sqrt{s_{NN}} = 2.76$ TeV. *Eur. J. Phys. C* **73**, 2617 (2013)
36. ALICE Collaboration, B.B. Abelev et al., J/ψ production and nuclear effects in p–Pb collisions at $\sqrt{s_{NN}} = 5.02$ TeV. *JHEP* **02**, 073 (2014). [arXiv:1308.6726](#) [nucl-ex]
37. ALICE Collaboration, B.B. Abelev et al., Measurement of visible cross sections in proton–lead collisions at $\sqrt{s_{NN}} = 5.02$ TeV in van der Meer scans with the ALICE detector. *JINST* **9**(11), P11003 (2014). [arXiv:1405.1849](#) [nucl-ex]
38. Particle Data Group Collaboration, K.A. Olive et al., Review of particle physics. *Chin. Phys. C* **38**, 090001 (2014)
39. LHCb Collaboration, R. Aaij et al., Exclusive J/ψ and $\psi(2S)$ production in pp collisions at $\sqrt{s} = 7$ TeV. *J. Phys. G* **40**, 045001 (2013). [arXiv:1301.7084](#) [hep-ex]
40. P. Newman, M. Wing, The hadronic final state at HERA. *Rev. Mod. Phys.* **86**(3), 1037 (2014). [arXiv:1308.3368](#) [hep-ex]
41. F. D. Aaron et al., Measurement of the inclusive ep scattering cross section at low Q^2 and x at HERA. *Eur. Phys. J. C* **63**(4), 625 (2009). <https://doi.org/10.1140/epjc/s10052-009-1128-6>
42. S.P. Jones, A.D. Martin, M.G. Ryskin, T. Teubner, Probes of the small x gluon via exclusive J/ψ and Υ production at HERA and the LHC. *JHEP* **11**, 085 (2013). [arXiv:1307.7099](#)
43. N. Armesto, A.H. Rezaeian, Exclusive vector meson production at high energies and gluon saturation. *Phys. Rev. D* **90**(5), 054003 (2014). [arXiv:1402.4831](#) [hep-ph]
44. I. Bautista, A. Fernández Tellez, M. Hentschinski, BFKL evolution and the growth with energy of exclusive J/ψ and Υ photoproduction cross sections. *Phys. Rev. D* **94**, 054002 (2016). <http://link.aps.org/doi/10.1103/PhysRevD.94.054002>
45. J. Cepila, J.G. Contreras, J.D. Tapia Takaki, Energy dependence of dissociative J/ψ photoproduction as a signature of gluon saturation at the LHC. *Phys. Lett. B* **766**, 186 (2017). [arXiv:1608.07559](#) [hep-ph]

ALICE Collaboration

S. Acharya¹³⁹, F. T. Acosta²⁰, J. Adam³⁷, D. Adamová⁹³, A. Adler⁷⁴, J. Adolfsson⁸⁰, M. M. Aggarwal⁹⁸, G. Aglieri Rinella³⁴, M. Agnello³¹, N. Agrawal⁴⁸, Z. Ahammed¹³⁹, S. U. Ahn⁷⁶, S. Aiola¹⁴⁴, A. Akindinov⁶⁴, M. Al-Turany¹⁰⁴, S. N. Alam¹³⁹, D. S. D. Albuquerque¹²¹, D. Aleksandrov⁸⁷, B. Alessandro⁵⁸, H. M. Alfanda⁶, R. Alfaro Molina⁷², Y. Ali¹⁵, A. Alici^{10,27,53}, A. Alkin², J. Alme²², T. Alt⁶⁹, L. Altenkamper²², I. Altsybeev¹¹¹, M. N. Anaam⁶, C. Andrei⁴⁷, D. Andreou³⁴, H. A. Andrews¹⁰⁸, A. Andronic^{104,142}, M. Angeletti³⁴, V. Anguelov¹⁰², C. Anson¹⁶, T. Antičić¹⁰⁵, F. Antinori⁵⁶, P. Antonioli⁵³, R. Anwar¹²⁵, N. Apadula⁷⁹, L. Aphecetche¹¹³, H. Appelshäuser⁶⁹, S. Arcelli²⁷, R. Arnaldi⁵⁸, M. Arratia⁷⁹, I. C. Arsene²¹, M. Arslanovic¹⁰², A. Augustinus³⁴, R. Averbeck¹⁰⁴, M. D. Azmi¹⁷, A. Badalà⁵⁵, Y. W. Baek^{40,60}, S. Bagnasco⁵⁸, R. Bailhache⁶⁹, R. Bala⁹⁹, A. Baldisseri¹³⁵, M. Ball⁴², R. C. Baral⁸⁵, A. M. Barbano²⁶, R. Barbera²⁸, F. Barile⁵², L. Barioglio²⁶, G. G. Barnaföldi¹⁴³, L. S. Barnby⁹², V. Barret¹³², P. Bartalini⁶, K. Barth³⁴, E. Bartsch⁶⁹, N. Bastid¹³², S. Basu¹⁴¹, G. Batigne¹¹³, B. Batyunya⁷⁵, P. C. Batzing²¹, J. L. Bazo Alba¹⁰⁹, I. G. Bearden⁸⁸, H. Beck¹⁰², C. Bedda⁶³, N. K. Behera⁶⁰, I. Belikov¹³⁴, F. Bellini³⁴, H. Bello Martinez⁴⁴, R. Bellwied¹²⁵, L. G. E. Beltran¹¹⁹, V. Belyaev⁹¹, G. Bencedi¹⁴³, S. Beole²⁶, A. Bercuci⁴⁷, Y. Berdnikov⁹⁶, D. Berenyi¹⁴³, R. A. Bertens¹²⁸, D. Berzano^{34,58}, L. Betev³⁴, P. P. Bhaduri¹³⁹, A. Bhasin⁹⁹, I. R. Bhat⁹⁹, H. Bhatt⁴⁸, B. Bhattacharjee⁴¹, J. Bhom¹¹⁷, A. Bianchi²⁶, L. Bianchi^{26,125}, N. Bianchi⁵¹, J. Bielčik³⁷, J. Bielčiková⁹³, A. Bilandzic^{103,116}, G. Biro¹⁴³, R. Biswas³, S. Biswas³, J. T. Blair¹¹⁸, D. Blau⁸⁷, C. Blume⁶⁹, G. Boca¹³⁷, F. Bock³⁴, A. Bogdanov⁹¹, L. Boldizsár¹⁴³, A. Bolozdynya⁹¹, M. Bombara³⁸, G. Bonomi¹³⁸, M. Bonora³⁴, H. Borel¹³⁵, A. Borissov^{102,142}, M. Borri¹²⁷, E. Botta²⁶, C. Bourjau⁸⁸, L. Bratrud⁶⁹, P. Braun-Munzinger¹⁰⁴, M. Bregant¹²⁰, T. A. Broker⁶⁹, M. Broz³⁷, E. J. Brucken⁴³, E. Bruna⁵⁸, G. E. Bruno^{33,34}, D. Budnikov¹⁰⁶, H. Buesching⁶⁹, S. Bufalino³¹, P. Buhler¹¹², P. Buncic³⁴, O. Busch^{131,a}, Z. Buthelezi⁷³, J. B. Butt¹⁵, J. T. Buxton⁹⁵, J. Cabala¹¹⁵, D. Caffarri⁸⁹, H. Caines¹⁴⁴, A. Caliva¹⁰⁴, E. Calvo Villar¹⁰⁹, R. S. Camacho⁴⁴, P. Camerini²⁵, A. A. Capon¹¹², W. Carena³⁴, F. Carnesecchi^{10,27}, J. Castillo Castellanos¹³⁵, A. J. Castro¹²⁸, E. A. R. Casula⁵⁴, C. Ceballos Sanchez⁸, S. Chandra¹³⁹, B. Chang¹²⁶, W. Chang⁶, S. Chapeland³⁴, M. Chartier¹²⁷, S. Chattopadhyay¹³⁹, S. Chattopadhyay¹⁰⁷, A. Chauvin²⁴, C. Cheshkov¹³³, B. Cheynis¹³³, V. Chibante Barroso³⁴, D. D. Chinellato¹²¹, S. Cho⁶⁰, P. Chochula³⁴, T. Chowdhury¹³², P. Christakoglou⁸⁹, C. H. Christensen⁸⁸, P. Christiansen⁸⁰, T. Chujo¹³¹, S. U. Chung¹⁸, C. Cicalo⁵⁴, L. Cifarelli^{10,27}, F. Cindolo⁵³, J. Cleymans¹²⁴, F. Colamaria⁵², D. Colella⁵², A. Collu⁷⁹, M. Colocci²⁷, M. Concas^{58,b}, G. Conesa Balbastre⁷⁸, Z. Conesa del Valle⁶¹, J. G. Contreras³⁷, T. M. Cormier⁹⁴, Y. Corrales Morales⁵⁸, P. Cortese³², M. R. Cosentino¹²², F. Costa³⁴, S. Costanza¹³⁷, J. Crkovaš⁶¹, P. Crochet¹³², E. Cuautle⁷⁰, L. Cunqueiro^{94,142}, D. Dabrowski¹⁴⁰, T. Dahms^{103,116}, A. Dainese⁵⁶, F. P. A. Damas^{113,135}, S. Dani⁶⁶, M. C. Danisch¹⁰², A. Danu⁶⁸, D. Das¹⁰⁷, I. Das¹⁰⁷, S. Das³, A. Dash⁸⁵, S. Dash⁴⁸, S. De⁴⁹, A. De Caro³⁰, G. de Cataldo⁵², C. de Conti¹²⁰, J. de Cuveland³⁹, A. De Falco²⁴, D. De Gruttola^{10,30}, N. De Marco⁵⁸, S. De Pasquale³⁰, R. D. De Souza¹²¹, H. F. Degenhardt¹²⁰, A. Deisting^{102,104}, A. Deloff⁸⁴, S. Delsanto²⁶, C. Deplano⁸⁹, P. Dhankher⁴⁸, D. Di Bari³³, A. Di Mauro³⁴, B. Di Ruzza⁵⁶, R. A. Diaz⁸, T. Dietel¹²⁴, P. Dillenseger⁶⁹, Y. Ding⁶, R. Divia³⁴, Ø. Djuvsland²², A. Dobrin³⁴, D. Domenicis Gimenez¹²⁰, B. Dönigus⁶⁹, O. Dordic²¹, A. K. Dubey¹³⁹, A. Dubla¹⁰⁴, L. Ducroux¹³³, S. Dudi⁹⁸, A. K. Duggal⁹⁸, M. Dukhishyam⁸⁵, P. Dupieux¹³², R. J. Ehlers¹⁴⁴, D. Elia⁵², E. Endress¹⁰⁹, H. Engel⁷⁴, E. Epple¹⁴⁴, B. Erazmus¹¹³, F. Erhardt⁹⁷, A. Erokhin¹¹¹, M. R. Ersdal²², B. Espagnon⁶¹, G. Eulisse³⁴, J. Eum¹⁸, D. Evans¹⁰⁸, S. Evdokimov⁹⁰, L. Fabbietti^{103,116}, M. Faggin²⁹, J. Faivre⁷⁸, A. Fantoni⁵¹, M. Fasel⁹⁴, L. Feldkamp¹⁴², A. Feliciello⁵⁸, G. Feofilov¹¹¹, A. Fernández Téllez⁴⁴, A. Ferretti²⁶, A. Festanti³⁴, V. J. G. Feuillard¹⁰², J. Figiel¹¹⁷, M. A. S. Figueredo¹²⁰, S. Filchagin¹⁰⁶, D. Finogeev⁶², F. M. Fionda²², G. Fiorenza⁵², F. Flor¹²⁵, M. Floris³⁴, S. Foertsch⁷³, P. Foka¹⁰⁴, S. Fokin⁸⁷, E. Fragiaco⁵⁹, A. Francescon³⁴, A. Francisco¹¹³, U. Frankenfeld¹⁰⁴, G. G. Fronze²⁶, U. Fuchs³⁴, C. Furget⁷⁸, A. Furs⁶², M. Fusco Girard³⁰, J. J. Gaardhøje⁸⁸, M. Gagliardi²⁶, A. M. Gago¹⁰⁹, K. Gajdosova⁸⁸, M. Gallio²⁶, C. D. Galvan¹¹⁹, P. Ganoti⁸³, C. Garabatos¹⁰⁴, E. Garcia-Solis¹¹, K. Garg²⁸, C. Gargiulo³⁴, K. Garner¹⁴², P. Gasik^{103,116}, E. F. Gauger¹¹⁸, M. B. Gay Ducati⁷¹, M. Germain¹¹³, J. Ghosh¹⁰⁷, P. Ghosh¹³⁹, S. K. Ghosh³, P. Gianotti⁵¹, P. Giubellino^{58,104}, P. Giubileo²⁹, P. Glässel¹⁰², D. M. Gómez Coral⁷², A. Gomez Ramirez⁷⁴, V. Gonzalez¹⁰⁴, P. González-Zamora⁴⁴, S. Gorbunov³⁹, L. Görlich¹¹⁷, S. Gotovac³⁵, V. Grabski⁷², L. K. Graczykowski¹⁴⁰, K. L. Graham¹⁰⁸, L. Greiner⁷⁹, A. Grelli⁶³, C. Grigoras³⁴, V. Grigoriev⁹¹, A. Grigoryan¹, S. Grigoryan⁷⁵, J. M. Gronefeld¹⁰⁴, F. Grosa³¹, J. F. Grosse-Oetringhaus³⁴, R. Grosso¹⁰⁴, R. Guernane⁷⁸, B. Guerzoni²⁷, M. Guittiere¹¹³, K. Gulbrandsen⁸⁸, T. Gunji¹³⁰, A. Gupta⁹⁹, R. Gupta⁹⁹, I. B. Guzman⁴⁴, R. Haake^{34,144}, M. K. Habib¹⁰⁴, C. Hadjidakis⁶¹, H. Hamagaki⁸¹, G. Hamar¹⁴³, M. Hamid⁶, J. C. Hamon¹³⁴, R. Hannigan¹¹⁸, M. R. Haque⁶³, J. W. Harris¹⁴⁴, A. Harton¹¹, H. Hassan⁷⁸, D. Hatzifotiadou^{10,53}, P. Hauer⁴², S. Hayashi¹³⁰, S. T. Heckel⁶⁹, E. Hellbär⁶⁹, H. Helstrup³⁶, A. Herghelegiu⁴⁷, E. G. Hernandez⁴⁴, G. Herrera Corral⁹, F. Herrmann¹⁴², K. F. Hetland³⁶, T. E. Hilden⁴³, H. Hillemanns³⁴, C. Hills¹²⁷, B. Hippolyte¹³⁴, B. Hohlweger¹⁰³, D. Horak³⁷, S. Hornung¹⁰⁴, R. Hosokawa^{78,131}, J. Hota⁶⁶, P. Hristov³⁴, C. Huang⁶¹, C. Hughes¹²⁸, P. Huhn⁶⁹, T. J. Humanic⁹⁵, H. Hushnud¹⁰⁷, N. Hussain⁴¹, T. Hussain¹⁷, D. Hutter³⁹, D. S. Hwang¹⁹

J. P. Iddon¹²⁷, R. Ilkaev¹⁰⁶, M. Inaba¹³¹, M. Ippolitov⁸⁷, M. S. Islam¹⁰⁷, M. Ivanov¹⁰⁴, V. Ivanov⁹⁶, V. Izucheev⁹⁰, B. Jacak⁷⁹, N. Jacazio²⁷, P. M. Jacobs⁷⁹, M. B. Jadhav⁴⁸, S. Jadlovská¹¹⁵, J. Jadlovsky¹¹⁵, S. Jaelani⁶³, C. Jahnke^{116,120}, M. J. Jakubowska¹⁴⁰, M. A. Janik¹⁴⁰, C. Jena⁸⁵, M. Jercic⁹⁷, O. Jevons¹⁰⁸, R. T. Jimenez Bustamante¹⁰⁴, M. Jin¹²⁵, P. G. Jones¹⁰⁸, A. Jusko¹⁰⁸, P. Kalinak⁶⁵, A. Kalweit³⁴, J. H. Kang¹⁴⁵, V. Kaplin⁹¹, S. Kar⁶, A. Karasu Uysal⁷⁷, O. Karavichev⁶², T. Karavicheva⁶², P. Karczmarczyk³⁴, E. Karpechev⁶², U. Kebschull⁷⁴, R. Keidel⁴⁶, D. L. D. Keijdener⁶³, M. Keil³⁴, B. Ketzer⁴², Z. Khabanova⁸⁹, A. M. Khan⁶, S. Khan¹⁷, S. A. Khan¹³⁹, A. Khanzadeev⁹⁶, Y. Kharlov⁹⁰, A. Khatun¹⁷, A. Khuntia⁴⁹, M. M. Kielbowicz¹¹⁷, B. Kileng³⁶, B. Kim¹³¹, D. Kim¹⁴⁵, D. J. Kim¹²⁶, E. J. Kim¹³, H. Kim¹⁴⁵, J. S. Kim⁴⁰, J. Kim¹⁰², J. Kim¹³, M. Kim^{60,102}, S. Kim¹⁹, T. Kim¹⁴⁵, T. Kim¹⁴⁵, K. Kindra⁹⁸, S. Kirsch³⁹, I. Kisel³⁹, S. Kiselev⁶⁴, A. Kisiel¹⁴⁰, J. L. Klay⁵, C. Klein⁶⁹, J. Klein⁵⁸, C. Klein-Bösing¹⁴², S. Klewin¹⁰², A. Kluge³⁴, M. L. Knichel³⁴, A. G. Knospe¹²⁵, C. Kobdaj¹¹⁴, M. Kofarago¹⁴³, M. K. Köhler¹⁰², T. Kollegger¹⁰⁴, N. Kondratyeva⁹¹, E. Kondratyuk⁹⁰, A. Konevskikh⁶², P. J. Konopka³⁴, M. Konyushikhin¹⁴¹, L. Koska¹¹⁵, O. Kovalenko⁸⁴, V. Kovalenko¹¹¹, M. Kowalski¹¹⁷, I. Králik⁶⁵, A. Kravčáková³⁸, L. Kreis¹⁰⁴, M. Krivda^{65,108}, F. Krizek⁹³, M. Krüger⁶⁹, E. Kryshen⁹⁶, M. Krzewicki³⁹, A. M. Kubera⁹⁵, V. Kučera^{60,93}, C. Kuhn¹³⁴, P. G. Kuijter⁸⁹, J. Kumar⁴⁸, L. Kumar⁹⁸, S. Kumar⁴⁸, S. Kundu⁸⁵, P. Kurashvili⁸⁴, A. Kurepin⁶², A. B. Kurepin⁶², S. Kushpil⁹³, J. Kvapil¹⁰⁸, M. J. Kweon⁶⁰, Y. Kwon¹⁴⁵, S. L. La Pointe³⁹, P. La Rocca²⁸, Y. S. Lai⁷⁹, I. Lakomov³⁴, R. Langoy¹²³, K. Lapidus¹⁴⁴, A. Lardeux²¹, P. Larionov⁵¹, E. Laudi³⁴, R. Lavicka³⁷, R. Lea²⁵, L. Leardini¹⁰², S. Lee¹⁴⁵, F. Lehas⁸⁹, S. Lehner¹¹², J. Lehrbach³⁹, R. C. Lemmon⁹², I. León Monzón¹¹⁹, P. Lévai¹⁴³, X. Li¹², X. L. Li⁶, J. Lien¹²³, R. Lietava¹⁰⁸, B. Lim¹⁸, S. Lindal²¹, V. Lindenstruth³⁹, S. W. Lindsay¹²⁷, C. Lippmann¹⁰⁴, M. A. Lisa⁹⁵, V. Litichevskiy⁴³, A. Liu⁷⁹, H. M. Ljunggren⁸⁰, W. J. Llope¹⁴¹, D. F. Lodato⁶³, V. Loginov⁹¹, C. Loizides^{79,94}, P. Loncar³⁵, X. Lopez¹³², E. López Torres⁸, P. Luettig⁶⁹, J. R. Luhder¹⁴², M. Lunardon²⁹, G. Luparello⁵⁹, M. Lupi³⁴, A. Maevskaya⁶², M. Mager³⁴, S. M. Mahmood²¹, A. Maire¹³⁴, R. D. Majka¹⁴⁴, M. Malaev⁹⁶, Q. W. Malik²¹, L. Malinina^{75,c}, D. Mal'Kevich⁶⁴, P. Malzacher¹⁰⁴, A. Mamonov¹⁰⁶, V. Manko⁸⁷, F. Manso¹³², V. Manzari⁵², Y. Mao⁶, M. Marchisone^{129,133}, J. Mareš⁶⁷, G. V. Margagliotti²⁵, A. Margotti⁵³, J. Margutti⁶³, A. Marín¹⁰⁴, C. Markert¹¹⁸, M. Marquard⁶⁹, N. A. Martin^{102,104}, P. Martinengo³⁴, J. L. Martinez¹²⁵, M. I. Martínez⁴⁴, G. Martínez García¹¹³, M. Martinez Pedreira³⁴, S. Masciocchi¹⁰⁴, M. Masera²⁶, A. Masoni⁵⁴, L. Massacrier⁶¹, E. Masson¹¹³, A. Mastroserio^{52,136}, A. M. Mathis^{103,116}, P. F. T. Matuoka¹²⁰, A. Matyja^{117,128}, C. Mayer¹¹⁷, M. Mazzilli³³, M. A. Mazzoni⁵⁷, F. Meddi²³, Y. Melikyan⁹¹, A. Menchaca-Rocha⁷², E. Meninno³⁰, M. Meres¹⁴, S. Mhlanga¹²⁴, Y. Miake¹³¹, L. Micheletti²⁶, M. M. Mieskolainen⁴³, D. L. Mihaylov¹⁰³, K. Mikhaylov^{64,75}, A. Mischke⁶³, A. N. Mishra⁷⁰, D. Miśkowiec¹⁰⁴, J. Mitra¹³⁹, C. M. Mitu⁶⁸, N. Mohammadi³⁴, A. P. Mohanty⁶³, B. Mohanty⁸⁵, M. Mohisin Khan^{17,d}, D. A. Moreira De Godoy¹⁴², L. A. P. Moreno⁴⁴, S. Moretto²⁹, A. Morreale¹¹³, A. Morsch³⁴, T. Mrnjavac³⁴, V. Muccifora⁵¹, E. Mudnic³⁵, D. Mühlheim¹⁴², S. Muhuri¹³⁹, M. Mukherjee³, J. D. Mulligan¹⁴⁴, M. G. Munhoz¹²⁰, K. Munning⁴², R. H. Munzer⁶⁹, H. Murakami¹³⁰, S. Murray⁷³, L. Musa³⁴, J. Musinsky⁶⁵, C. J. Myers¹²⁵, J. W. Myrcha¹⁴⁰, B. Naik⁴⁸, R. Nair⁸⁴, B. K. Nandi⁴⁸, R. Nania^{10,53}, E. Nappi⁵², A. Narayan⁴⁸, M. U. Naru¹⁵, A. F. Nassirpour⁸⁰, H. Natal da Luz¹²⁰, C. Nattrass¹²⁸, S. R. Navarro⁴⁴, K. Nayak⁸⁵, R. Nayak⁴⁸, T. K. Nayak¹³⁹, S. Nazarenko¹⁰⁶, R. A. Negrao De Oliveira^{34,69}, L. Nellen⁷⁰, S. V. Nesbo³⁶, G. Neskovic³⁹, F. Ng¹²⁵, M. Nicassio¹⁰⁴, J. Niedziela^{34,140}, B. S. Nielsen⁸⁸, S. Nikolaev⁸⁷, S. Nikulin⁸⁷, V. Nikulin⁹⁶, F. Noferini^{10,53}, P. Nomokonov⁷⁵, G. Nooren⁶³, J. C. C. Noris⁴⁴, J. Norman⁷⁸, A. Nyanin⁸⁷, J. Nystrand²², M. Ogino⁸¹, H. Oh¹⁴⁵, A. Ohlson¹⁰², J. Oleniacz¹⁴⁰, A. C. Oliveira Da Silva¹²⁰, M. H. Oliver¹⁴⁴, J. Onderwaater¹⁰⁴, C. Oppedisano⁵⁸, R. Orava⁴³, M. Oravec¹¹⁵, A. Ortiz Velasquez⁷⁰, A. Oskarsson⁸⁰, J. Otwinowski¹¹⁷, K. Oyama⁸¹, Y. Pachmayer¹⁰², V. Pacik⁸⁸, D. Pagano¹³⁸, G. Paic⁷⁰, P. Palni⁶, J. Pan¹⁴¹, A. K. Pandey⁴⁸, S. Panebianco¹³⁵, V. Papikyan¹, P. Pareek⁴⁹, J. Park⁶⁰, J. E. Parkkila¹²⁶, S. Parmar⁹⁸, A. Passfeld¹⁴², S. P. Pathak¹²⁵, R. N. Patra¹³⁹, B. Paul⁵⁸, H. Pei⁶, T. Peitzmann⁶³, X. Peng⁶, L. G. Pereira⁷¹, H. Pereira Da Costa¹³⁵, D. Peresunko⁸⁷, E. Perez Lezama⁶⁹, V. Peskov⁶⁹, Y. Pestov⁴, V. Petráček³⁷, M. Petrovici⁴⁷, C. Petta²⁸, R. P. Pezzi⁷¹, S. Piano⁵⁹, M. Pikna¹⁴, P. Pillot¹¹³, L. O. D. L. Pimentel⁸⁸, O. Pinazza^{34,53}, L. Pinsky¹²⁵, S. Pisano⁵¹, D. B. Piyarathna¹²⁵, M. Płoskoń⁷⁹, M. Planinic⁹⁷, F. Pliquetti⁶⁹, J. Pluta¹⁴⁰, S. Pochybova¹⁴³, P. L. M. Podesta-Lerma¹¹⁹, M. G. Poghosyan⁹⁴, B. Polichtchouk⁹⁰, N. Poljak⁹⁷, W. Poonsawat¹¹⁴, A. Pop⁴⁷, H. Poppenborg¹⁴², S. Porteboeuf-Houssais¹³², V. Pozdniakov⁷⁵, S. K. Prasad³, R. Preghenella⁵³, F. Prino⁵⁸, C. A. Pruneau¹⁴¹, I. Pshenichnov⁶², M. Puccio²⁶, V. Punin¹⁰⁶, K. Puranapanda¹³⁹, J. Putschke¹⁴¹, S. Raha³, S. Rajput⁹⁹, J. Rak¹²⁶, A. Rakotozafindrabe¹³⁵, L. Ramello³², F. Rami¹³⁴, R. Raniwala¹⁰⁰, S. Raniwala¹⁰⁰, S. S. Räsänen⁴³, B. T. Rascanu⁶⁹, R. Rath⁴⁹, V. Ratza⁴², I. Ravasenga³¹, K. F. Read^{94,128}, K. Redlich^{84,e}, A. Rehman²², P. Reichelt⁶⁹, F. Reidt³⁴, X. Ren⁶, R. Renfordt⁶⁹, A. Reshetin⁶², J.-P. Revol¹⁰, K. Reygers¹⁰², V. Riabov⁹⁶, T. Richert^{63,80,88}, M. Richter²¹, P. Riedler³⁴, W. Riegler³⁴, F. Riggi²⁸, C. Ristea⁶⁸, S. P. Rode⁴⁹, M. Rodríguez Cahuantzi⁴⁴, K. Røed²¹, R. Rogalev⁹⁰, E. Rogochaya⁷⁵, D. Rohr³⁴, D. Röhrich²², P. S. Rokita¹⁴⁰, F. Ronchetti⁵¹, E. D. Rosas⁷⁰, K. Roslon¹⁴⁰, P. Rosnet¹³², A. Rossi^{29,56}, A. Rotondi¹³⁷, F. Roukoutakis⁸³, C. Roy¹³⁴, P. Roy¹⁰⁷, O. V. Rueda⁷⁰, R. Rui²⁵, B. Rumyantsev⁷⁵, A. Rustamov⁸⁶, E. Ryabinkin⁸⁷, Y. Ryabov⁹⁶, A. Rybicki¹¹⁷, S. Saarinen⁴³, S. Sadhu¹³⁹, S. Sadovsky⁹⁰, K. Šafařík³⁴, S. K. Saha¹³⁹, B. Sahoo⁴⁸, P. Sahoo⁴⁹, R. Sahoo⁴⁹, S. Sahoo⁶⁶, P. K. Sahu⁶⁶, J. Saini¹³⁹

S. Sakai¹³¹, M. A. Saleh¹⁴¹, S. Sambyal⁹⁹, V. Samsonov^{91,96}, A. Sandoval⁷², A. Sarkar⁷³, D. Sarkar¹³⁹, N. Sarkar¹³⁹, P. Sarma⁴¹, M. H. P. Sas⁶³, E. Scapparone⁵³, F. Scarlassara²⁹, B. Schaefer⁹⁴, H. S. Scheid⁶⁹, C. Schiaua⁴⁷, R. Schicker¹⁰², C. Schmidt¹⁰⁴, H. R. Schmidt¹⁰¹, M. O. Schmidt¹⁰², M. Schmidt¹⁰¹, N. V. Schmidt^{69,94}, J. Schukraft³⁴, Y. Schutz^{34,134}, K. Schwarz¹⁰⁴, K. Schweda¹⁰⁴, G. Scioli²⁷, E. Scomparin⁵⁸, M. Šefčík³⁸, J. E. Seger¹⁶, Y. Sekiguchi¹³⁰, D. Sekihata⁴⁵, I. Selyuzhenkov^{91,104}, S. Senyukov¹³⁴, E. Serradilla⁷², P. Sett⁴⁸, A. Sevcenco⁶⁸, A. Shabanov⁶², A. Shabetai¹¹³, R. Shahoyan³⁴, W. Shaikh¹⁰⁷, A. Shangaraev⁹⁰, A. Sharma⁹⁸, A. Sharma⁹⁹, M. Sharma⁹⁹, N. Sharma⁹⁸, A. I. Sheikh¹³⁹, K. Shigaki⁴⁵, M. Shimomura⁸², S. Shirinkin⁶⁴, Q. Shou^{6,110}, Y. Sibiriak⁸⁷, S. Siddhanta⁵⁴, K. M. Sielewicz³⁴, T. Siemiarczuk⁸⁴, D. Silvermyr⁸⁰, G. Simatovic⁸⁹, G. Simonetti^{34,103}, R. Singaraju¹³⁹, R. Singh⁸⁵, R. Singh⁹⁹, V. Singhal¹³⁹, T. Sinha¹⁰⁷, B. Sitar¹⁴, M. Sitta³², T. B. Skaali²¹, M. Slupecki¹²⁶, N. Smirnov¹⁴⁴, R. J. M. Snellings⁶³, T. W. Snellman¹²⁶, J. Sochan¹¹⁵, C. Soncco¹⁰⁹, J. Song^{18,60}, A. Songmoolnak¹¹⁴, F. Soramel²⁹, S. Sorensen¹²⁸, F. Sozzi¹⁰⁴, I. Sputowska¹¹⁷, J. Stachel¹⁰², I. Stan⁶⁸, P. Stankus⁹⁴, E. Stenlund⁸⁰, D. Stocco¹¹³, M. M. Storetvedt³⁶, P. Strmen¹⁴, A. A. P. Suaide¹²⁰, T. Sugitate⁴⁵, C. Suire⁶¹, M. Suleymanov¹⁵, M. Suljic³⁴, R. Sultanov⁶⁴, M. Šumbera⁹³, S. Sumowidagdo⁵⁰, K. Suzuki¹¹², S. Swain⁶⁶, A. Szabo¹⁴, I. Szarka¹⁴, U. Tabassam¹⁵, J. Takahashi¹²¹, G. J. Tambave²², N. Tanaka¹³¹, M. Tarhini¹¹³, M. G. Tarzila⁴⁷, J. D. Tapia Takaki⁶¹, A. Tauro³⁴, G. Tejeda Muñoz⁴⁴, A. Telesca³⁴, C. Terrevoli²⁹, B. Teyssier¹³³, D. Thakur⁴⁹, S. Thakur¹³⁹, D. Thomas¹¹⁸, F. Thoresen⁸⁸, R. Tieulent¹³³, A. Tikhonov⁶², A. R. Timmins¹²⁵, A. Toia⁶⁹, N. Topilskaya⁶², M. Toppi⁵¹, S. R. Torres¹¹⁹, S. Tripathy⁴⁹, S. Trogolo²⁶, G. Trombetta³³, L. Tropp³⁸, V. Trubnikov², W. H. Trzaska¹²⁶, T. P. Trzcinski¹⁴⁰, B. A. Trzeciak⁶³, T. Tsuji¹³⁰, A. Tumkin¹⁰⁶, R. Turrisi⁵⁶, T. S. Tveter²¹, K. Ullaland²², E. N. Umaka¹²⁵, A. Uras¹³³, G. L. Usai²⁴, A. Utrobicic⁹⁷, M. Vala¹¹⁵, L. Valencia Palomo⁴⁴, N. Valle¹³⁷, N. van der Kolk⁶³, L. V. R. van Doremalen⁶³, J. W. Van Hoorne³⁴, M. van Leeuwen⁶³, P. Vande Vyvre³⁴, D. Varga¹⁴³, A. Vargas⁴⁴, M. Vargyas¹²⁶, R. Varma⁴⁸, M. Vasileiou⁸³, A. Vasiliev⁸⁷, O. Vázquez Doce^{103,116}, V. Vechernin¹¹¹, A. M. Veen⁶³, E. Vercellin²⁶, S. Vergara Limón⁴⁴, L. Vermunt⁶³, R. Vernet⁷, R. Vértesi¹⁴³, L. Vickovic³⁵, J. Viinikainen¹²⁶, Z. Vilakazi¹²⁹, O. Villalobos Baillie¹⁰⁸, A. Villatoro Tello⁴⁴, A. Vinogradov⁸⁷, T. Virgili³⁰, V. Vislavicius^{80,88}, A. Vodopyanov⁷⁵, M. A. Völkl¹⁰¹, K. Voloshin⁶⁴, S. A. Voloshin¹⁴¹, G. Volpe³³, B. von Haller³⁴, I. Vorobyev^{103,116}, D. Voscek¹¹⁵, D. Vranic^{34,104}, J. Vrláková³⁸, B. Wagner²², M. Wang⁶, Y. Watanabe¹³¹, M. Weber¹¹², S. G. Weber¹⁰⁴, A. Wegrzynek³⁴, D. F. Weiser¹⁰², S. C. Wenzel³⁴, J. P. Wessels¹⁴², U. Westerhoff¹⁴², A. M. Whitehead¹²⁴, J. Wiechula⁶⁹, J. Wikne²¹, G. Wilk⁸⁴, J. Wilkinson⁵³, G. A. Willems^{34,142}, M. C. S. Williams⁵³, E. Willsher¹⁰⁸, B. Windelband¹⁰², W. E. Witt¹²⁸, R. Xu⁶, S. Yalcin⁷⁷, K. Yamakawa⁴⁵, S. Yano^{45,135}, Z. Yin⁶, H. Yokoyama^{78,131}, I.-K. Yoo¹⁸, J. H. Yoon⁶⁰, S. Yuan²², V. Yurchenko², V. Zaccolo⁵⁸, A. Zaman¹⁵, C. Zampolli³⁴, H. J. C. Zanoli¹²⁰, N. Zardoshti¹⁰⁸, A. Zarochentsev¹¹¹, P. Závada⁶⁷, N. Zaviyalov¹⁰⁶, H. Zbroszczyk¹⁴⁰, M. Zhalov⁹⁶, X. Zhang⁶, Y. Zhang⁶, Z. Zhang^{6,132}, C. Zhao²¹, V. Zhrebchevskii¹¹¹, N. Zhigareva⁶⁴, D. Zhou⁶, Y. Zhou⁸⁸, Z. Zhou²², H. Zhu⁶, J. Zhu⁶, Y. Zhu⁶, A. Zichichi^{10,27}, M. B. Zimmermann³⁴, G. Zinovjev², J. Zmeskal¹¹²

- ¹ A.I. Alikhanyan National Science Laboratory (Yerevan Physics Institute) Foundation, Yerevan, Armenia
- ² Bogolyubov Institute for Theoretical Physics, National Academy of Sciences of Ukraine, Kiev, Ukraine
- ³ Bose Institute, Department of Physics and Centre for Astroparticle Physics and Space Science (CAPSS), Kolkata, India
- ⁴ Budker Institute for Nuclear Physics, Novosibirsk, Russia
- ⁵ California Polytechnic State University, San Luis Obispo, CA, USA
- ⁶ Central China Normal University, Wuhan, China
- ⁷ Centre de Calcul de l'IN2P3, Villeurbanne, Lyon, France
- ⁸ Centro de Aplicaciones Tecnológicas y Desarrollo Nuclear (CEADEN), Havana, Cuba
- ⁹ Centro de Investigación y de Estudios Avanzados (CINVESTAV), Mexico City and Mérida, Mexico
- ¹⁰ Centro Fermi-Museo Storico della Fisica e Centro Studi e Ricerche "Enrico Fermi", Rome, Italy
- ¹¹ Chicago State University, Chicago, IL, USA
- ¹² China Institute of Atomic Energy, Beijing, China
- ¹³ Chonbuk National University, Jeonju, Republic of Korea
- ¹⁴ Comenius University Bratislava, Faculty of Mathematics, Physics and Informatics, Bratislava, Slovakia
- ¹⁵ COMSATS Institute of Information Technology (CIIT), Islamabad, Pakistan
- ¹⁶ Creighton University, Omaha, NE, USA
- ¹⁷ Department of Physics, Aligarh Muslim University, Aligarh, India
- ¹⁸ Department of Physics, Pusan National University, Pusan, Republic of Korea
- ¹⁹ Department of Physics, Sejong University, Seoul, Republic of Korea
- ²⁰ Department of Physics, University of California, Berkeley, CA, USA
- ²¹ Department of Physics, University of Oslo, Oslo, Norway

- 22 Department of Physics and Technology, University of Bergen, Bergen, Norway
- 23 Dipartimento di Fisica dell'Università 'La Sapienza' and Sezione INFN, Rome, Italy
- 24 Dipartimento di Fisica dell'Università and Sezione INFN, Cagliari, Italy
- 25 Dipartimento di Fisica dell'Università and Sezione INFN, Trieste, Italy
- 26 Dipartimento di Fisica dell'Università and Sezione INFN, Turin, Italy
- 27 Dipartimento di Fisica e Astronomia dell'Università and Sezione INFN, Bologna, Italy
- 28 Dipartimento di Fisica e Astronomia dell'Università and Sezione INFN, Catania, Italy
- 29 Dipartimento di Fisica e Astronomia dell'Università and Sezione INFN, Padova, Italy
- 30 Dipartimento di Fisica 'E.R. Caianiello' dell'Università and Gruppo Collegato INFN, Salerno, Italy
- 31 Dipartimento DISAT del Politecnico and Sezione INFN, Turin, Italy
- 32 Dipartimento di Scienze e Innovazione Tecnologica dell'Università del Piemonte Orientale and INFN Sezione di Torino, Alessandria, Italy
- 33 Dipartimento Interateneo di Fisica 'M. Merlin' and Sezione INFN, Bari, Italy
- 34 European Organization for Nuclear Research (CERN), Geneva, Switzerland
- 35 Faculty of Electrical Engineering, Mechanical Engineering and Naval Architecture, University of Split, Split, Croatia
- 36 Faculty of Engineering and Science, Western Norway University of Applied Sciences, Bergen, Norway
- 37 Faculty of Nuclear Sciences and Physical Engineering, Czech Technical University in Prague, Prague, Czech Republic
- 38 Faculty of Science, P.J. Šafárik University, Košice, Slovakia
- 39 Frankfurt Institute for Advanced Studies, Johann Wolfgang Goethe-Universität Frankfurt, Frankfurt, Germany
- 40 Gangneung-Wonju National University, Gangneung, Republic of Korea
- 41 Department of Physics, Gauhati University, Guwahati, India
- 42 Helmholtz-Institut für Strahlen- und Kernphysik, Rheinische Friedrich-Wilhelms-Universität Bonn, Bonn, Germany
- 43 Helsinki Institute of Physics (HIP), Helsinki, Finland
- 44 High Energy Physics Group, Universidad Autónoma de Puebla, Puebla, Mexico
- 45 Hiroshima University, Hiroshima, Japan
- 46 Hochschule Worms, Zentrum für Technologietransfer und Telekommunikation (ZTT), Worms, Germany
- 47 Horia Hulubei National Institute of Physics and Nuclear Engineering, Bucharest, Romania
- 48 Indian Institute of Technology Bombay (IIT), Mumbai, India
- 49 Indian Institute of Technology Indore, Indore, India
- 50 Indonesian Institute of Sciences, Jakarta, Indonesia
- 51 INFN, Laboratori Nazionali di Frascati, Frascati, Italy
- 52 INFN, Sezione di Bari, Bari, Italy
- 53 INFN, Sezione di Bologna, Bologna, Italy
- 54 INFN, Sezione di Cagliari, Cagliari, Italy
- 55 INFN, Sezione di Catania, Catania, Italy
- 56 INFN, Sezione di Padova, Padova, Italy
- 57 INFN, Sezione di Roma, Rome, Italy
- 58 INFN, Sezione di Torino, Turin, Italy
- 59 INFN, Sezione di Trieste, Trieste, Italy
- 60 Inha University, Incheon, Republic of Korea
- 61 Institut de Physique Nucléaire d'Orsay (IPNO), Institut National de Physique Nucléaire et de Physique des Particules (IN2P3/CNRS), Université Paris-Sud, Université Paris-Saclay, Orsay, France
- 62 Institute for Nuclear Research, Academy of Sciences, Moscow, Russia
- 63 Institute for Subatomic Physics, Utrecht University/Nikhef, Utrecht, Netherlands
- 64 Institute for Theoretical and Experimental Physics, Moscow, Russia
- 65 Institute of Experimental Physics, Slovak Academy of Sciences, Košice, Slovakia
- 66 Institute of Physics, Homi Bhabha National Institute, Bhubaneswar, India
- 67 Institute of Physics of the Czech Academy of Sciences, Prague, Czech Republic
- 68 Institute of Space Science (ISS), Bucharest, Romania
- 69 Institut für Kernphysik, Johann Wolfgang Goethe-Universität Frankfurt, Frankfurt, Germany
- 70 Instituto de Ciencias Nucleares, Universidad Nacional Autónoma de México, Mexico City, Mexico
- 71 Instituto de Física, Universidade Federal do Rio Grande do Sul (UFRGS), Porto Alegre, Brazil
- 72 Instituto de Física, Universidad Nacional Autónoma de México, Mexico City, Mexico

- 73 iThemba LABS, National Research Foundation, Somerset West, South Africa
- 74 Johann-Wolfgang-Goethe Universität Frankfurt Institut für Informatik, Fachbereich Informatik und Mathematik, Frankfurt, Germany
- 75 Joint Institute for Nuclear Research (JINR), Dubna, Russia
- 76 Korea Institute of Science and Technology Information, Daejeon, Republic of Korea
- 77 KTO Karatay University, Konya, Turkey
- 78 Laboratoire de Physique Subatomique et de Cosmologie, Université Grenoble-Alpes, CNRS-IN2P3, Grenoble, France
- 79 Lawrence Berkeley National Laboratory, Berkeley, CA, USA
- 80 Lund University Department of Physics, Division of Particle Physics, Lund, Sweden
- 81 Nagasaki Institute of Applied Science, Nagasaki, Japan
- 82 Nara Women's University (NWU), Nara, Japan
- 83 Department of Physics, National and Kapodistrian University of Athens, School of Science, Athens, Greece
- 84 National Centre for Nuclear Research, Warsaw, Poland
- 85 National Institute of Science Education and Research, Homi Bhabha National Institute, Jatni, India
- 86 National Nuclear Research Center, Baku, Azerbaijan
- 87 National Research Centre Kurchatov Institute, Moscow, Russia
- 88 Niels Bohr Institute, University of Copenhagen, Copenhagen, Denmark
- 89 Nikhef, National Institute for Subatomic Physics, Amsterdam, The Netherlands
- 90 NRC Kurchatov Institute IHEP, Protvino, Russia
- 91 NRNU Moscow Engineering Physics Institute, Moscow, Russia
- 92 Nuclear Physics Group, STFC Daresbury Laboratory, Daresbury, United Kingdom
- 93 Nuclear Physics Institute of the Czech Academy of Sciences, Řež u Prahy, Czech Republic
- 94 Oak Ridge National Laboratory, Oak Ridge, TN, USA
- 95 Ohio State University, Columbus, OH, USA
- 96 Petersburg Nuclear Physics Institute, Gatchina, Russia
- 97 Physics Department, Faculty of science, University of Zagreb, Zagreb, Croatia
- 98 Physics Department, Panjab University, Chandigarh, India
- 99 Physics Department, University of Jammu, Jammu, India
- 100 Physics Department, University of Rajasthan, Jaipur, India
- 101 Physikalisches Institut, Eberhard Karls Universität Tübingen, Tübingen, Germany
- 102 Physikalisches Institut, Ruprecht-Karls-Universität Heidelberg, Heidelberg, Germany
- 103 Physik Department, Technische Universität München, Munich, Germany
- 104 Research Division and ExtreMe Matter Institute EMMI, GSI Helmholtzzentrum für Schwerionenforschung GmbH, Darmstadt, Germany
- 105 Rudjer Bošković Institute, Zagreb, Croatia
- 106 Russian Federal Nuclear Center (VNIIEF), Sarov, Russia
- 107 Saha Institute of Nuclear Physics, Homi Bhabha National Institute, Kolkata, India
- 108 School of Physics and Astronomy, University of Birmingham, Birmingham, United Kingdom
- 109 Sección Física, Departamento de Ciencias, Pontificia Universidad Católica del Perú, Lima, Peru
- 110 Shanghai Institute of Applied Physics, Shanghai, China
- 111 St. Petersburg State University, St. Petersburg, Russia
- 112 Stefan Meyer Institut für Subatomare Physik (SMI), Vienna, Austria
- 113 SUBATECH, IMT Atlantique, Université de Nantes, CNRS-IN2P3, Nantes, France
- 114 Suranaree University of Technology, Nakhon, Ratchasima, Thailand
- 115 Technical University of Košice, Košice, Slovakia
- 116 Technische Universität München, Excellence Cluster 'Universe', Munich, Germany
- 117 The Henryk Niewodniczanski Institute of Nuclear Physics, Polish Academy of Sciences, Cracow, Poland
- 118 The University of Texas at Austin, Austin, TX, USA
- 119 Universidad Autónoma de Sinaloa, Culiacán, Mexico
- 120 Universidade de São Paulo (USP), São Paulo, Brazil
- 121 Universidade Estadual de Campinas (UNICAMP), Campinas, Brazil
- 122 Universidade Federal do ABC, Santo Andre, Brazil
- 123 University College of Southeast Norway, Tonsberg, Norway

- 124 University of Cape Town, Cape Town, South Africa
125 University of Houston, Houston, TX, USA
126 University of Jyväskylä, Jyväskylä, Finland
127 University of Liverpool, Liverpool, United Kingdom
128 University of Tennessee, Knoxville, TN, USA
129 University of the Witwatersrand, Johannesburg, South Africa
130 University of Tokyo, Tokyo, Japan
131 University of Tsukuba, Tsukuba, Japan
132 Université Clermont Auvergne, CNRS/IN2P3, LPC, Clermont-Ferrand, France
133 Université de Lyon, Université Lyon 1, CNRS/IN2P3, IPN-Lyon, Villeurbanne, Lyon, France
134 Université de Strasbourg, CNRS, IPHC UMR 7178, 67000 Strasbourg, France
135 Département de Physique Nucléaire (DPhN), Université Paris-Saclay Centre d'Études de Saclay (CEA), IRFU, Saclay, France
136 Università degli Studi di Foggia, Foggia, Italy
137 Università degli Studi di Pavia and Sezione INFN, Pavia, Italy
138 Università di Brescia and Sezione INFN, Brescia, Italy
139 Variable Energy Cyclotron Centre, Homi Bhabha National Institute, Kolkata, India
140 Warsaw University of Technology, Warsaw, Poland
141 Wayne State University, Detroit, MI, USA
142 Westfälische Wilhelms-Universität Münster, Institut für Kernphysik, Münster, Germany
143 Wigner Research Centre for Physics, Hungarian Academy of Sciences, Budapest, Hungary
144 Yale University, New Haven, CT, USA
145 Yonsei University, Seoul, Republic of Korea
- ^a Deceased
^b Dipartimento DET del Politecnico di Torino, Turin, Italy
^c M.V. Lomonosov Moscow State University, D.V. Skobeltsyn Institute of Nuclear Physics, Moscow, Russia
^d Department of Applied Physics, Aligarh Muslim University, Aligarh, India
^e Institute of Theoretical Physics, University of Wrocław, Poland